This article has been accepted for publication in a future issue of this journal, but has not been fully edited. Content may change prior to final publication. Citation information: DOI 10.1109/TVT.2018.2794322, IEEE Transactions on Vehicular Technology

Joint Azimuth, Elevation, and Delay Estimation for 3D Indoor Localization

Fei Wen, *Member*, *IEEE*, Peilin Liu, *Member*, *IEEE*, Haichao Wei, Yi Zhang, and Robert C. Qiu, *Fellow*, *IEEE*

***Abstract*—Accurate localization in harsh indoor environments has long been a challenging problem due to the presence of multipath. Since joint direction-of-arrival (DOA) and time delay (TD) estimation has the capability to separate the line-of-sight (LOS) signal from multipath signals in the TD space, it recently becomes a key technique for accurate indoor localization in next generation WiFi and 5G networks. This paper addresses the problem of joint azimuth, elevation and TD estimation of multiple reflections of a known signal. First, we propose an efficient approximate maximum likelihood (AML) algorithm for this problem, which updates the DOA and TD parameters alternatingly. This algorithm applies to arbitrarily distributed (planar or 3D) arrays. Then, we present closed-form Cramer-Rao bound (CRB) for joint DOA and TD estimation, based on which we provide further analysis to show the benefit of joint DOA and TD estimation over DOA-only estimation. Although the benefit of joint estimation has been empirically shown long ago, our analysis is the first theoretical proof of it. Finally, simulation results have been provided to demonstrate the theoretical finding and the effectiveness of the new algorithm. Matlab code for the new algorithm is available at https://github.com/FWen/JADE.git.**

***Index Terms*—Direction-of-arrival estimation, time delay estimation, maximum likelihood, Cramer-Rao bound, multipath, indoor localization, channel state information.**

I. Introduction

Accurate localization is of great importance in many emerging commercial and public safety applications, such as augmented reality, social networking, and retail shopping [1], [2], [37], [38]. Although accurate localization in harsh indoor environments has long been a challenging problem due to the presence of multipath and nonline-of-sight (NLOS) propagation [40], it is commonly expected to be achieved in next generation WiFi and 5G mobile communication networks [3]–[6]. Specifically, in next generation WiFi and 5G networks, two favorable opportunities arise for achieving high-accuracy indoor localization. First, WiFi access points and 5G base stations are incorporating ever-increasing numbers of antennas to bolster capacity and coverage with multiple-input multiple-output (MIMO) techniques. Second, the used signals have wider bandwidth (e.g., towards one hundred MHz or even more). More antennas facilitate accurate direction-of-arrival (DOA) estimation. Meanwhile, wider bandwidth facilitates accurate time delay (TD) estimation and, more importantly, facilitates reliable separation of the line-of-sight (LOS) signal from multipath signals. In this context, joint azimuth, elevation angles and TD estimation becomes a key technique for high-accuracy 3-dimensional (3D) indoor localization in next generation WiFi and 5G networks [7]–[9].

In the past two decades, a number of methods for joint DOA and TD estimation have been proposed, e.g., [10]–[23], [39] and references therein. For example, maximum likelihood (ML) methods have been developed in [10], [22], whilst more efficient subspace-based methods have been proposed in [11]–[21]. Compared with traditional DOA-only estimation methods (e.g., [24]–[26], [41]), joint DOA and TD estimation methods have shown significant superiority, since such methods fully exploit the spatial diversity as well as temporal diversity in estimating the multipath channel.

While the above works consider joint azimuth and TD estimation, this work addresses the joint azimuth, elevation and TD estimation problem. Generally, simultaneous estimation of the azimuth, elevation angles and TDs is far more complicated than joint azimuth and elevation estimation or joint azimuth and TD estimation, because the two angles and the delay need to be estimated jointly. For this problem, a MUSIC-like method has been proposed in [27], which requires a 3D search of the 3D MUSIC spectrum. More efficient subspace based methods have been proposed in [28], [29], but they are restricted to special arrays, e.g., uniform rectangular planar array [28] and uniform circular array (UCA) [29]. In comparison, the proposed approximate maximum likelihood (AML) method in this work is more efficient and applies to arbitrarily distributed (planar or 3D) arrays. Moreover, unlike [27], the CRB is provided in closed-form and concentrated to the DOA-block and TD-block, which facilitates further analysis. The main contributions of this work are as follows.

A. Contributions

First, we propose an efficient AML algorithm, which iteratively update the DOA (azimuth and elevation) and TD parameters in an alternating manner.

Second, the CRB for joint azimuth, elevation and TD estimation has been provided in closed-form, based on which we provide further analysis to show the advantage of joint DOA and TD estimation over DOA-only estimation. Although such advantage has been empirically shown long ago, our analysis is the first theoretical proof of it. The main results are as follows.

1) The DOA-related CRB for joint DOA and TD estimation is upper bounded by the associated CRB for DOA-only

This work was supported in part by the National Natural Science Foundation of China (NSFC) under grants 61401501 and 61472442.

F. Wen, P. Liu, and R. C. Qiu are with the Department of Electronic Engineering, Shanghai Jiao Tong University, Shanghai 200240, China (e-mail: wenfei@sjtu.edu.cn; liupeilin@sjtu.edu.cn; rcqiu@sjtu.edu.cn).

H. Wei and Y. Zhang is with Huawei Technologies Co., Ltd, Shanghai, China, (e-mail: weihaichao@huawei.com, aaabear@huawei.com).

This article has been accepted for publication in a future issue of this journal, but has not been fully edited. Content may change prior to final publication. Citation information: DOI 10.1109/TVT.2018.2794322, IEEE Transactions on Vehicular Technology

estimation. Further, in some special conditions, e.g., all the multipath signals have the same delay and/or there exists only a single path, these two CRBs are equivalent.

2) DOA overlapped signals (or signals with DOAs too close to be resolved by DOA-only estimation) can be resolved in the TD space via joint DOA and TD estimation, and vice versa.

3) For joint DOA and TD estimation, both the CRBs for DOA and TD are non-increasing functions with respect to the signal bandwidth.

Finally, we have evaluated the new algorithm and theoretical funding via various simulations.

B. Outline and Notations

The rest of this paper is organized as follows. Section II introduces the signal model and the Gaussian ML estimator. In Section III, we detail the new AML algorithm. Section IV contains the CRB for joint azimuth, elevation and TD estimation, and provides some analysis based on the CRB. Section V contains experimental results. Finally, Section VI ends the paper with concluding remarks.

Notations: $(\cdot)^*$, $(\cdot)^T$, and $(\cdot)^H$ denote the conjugate, transpose and Hermitian transpose, respectively. $\|\cdot\|^2$, $E(\cdot)$, $\det(\cdot)$, $\mathrm{Tr}(\cdot)$, $\Re(\cdot)$ and $\Im(\cdot)$ stand for the norm, expectation, determinant, trace, and real and imaginary part operators, respectively. $\mathbf{I}_M$ and $\mathbf{0}_M$ stand for $M \times M$ identity and zero matrices, respectively. $\mathbf{1}_M$ stands for an $M \times 1$ vector with each element be unit. For a vector $\mathbf{v}$, $\mathrm{diag}(\mathbf{v})$ is a diagonal matrix with diagonal elements be $\mathbf{v}$. $\mathrm{blkdiag}(\mathbf{M}_1, \cdots, \mathbf{M}_n)$ is a block-diagonal matrix with $\mathbf{M}_1, \cdots, \mathbf{M}_n$ on the diagonal. $\odot$ denotes the Hadamard product. $\mathbf{M} \geq \mathbf{0}$ means that $\mathbf{M}$ is positive-semidefinite. $\mathrm{rank}(\mathbf{M})$ denotes the rank of the matrix $\mathbf{M}$.

II. Signal Model and Maximum Likelihood Estimator

In this section, we introduce the signal model and present the Gaussian ML estimator.

A. Signal Model

Consider an M sensor arbitrarily distributed (2D planar or 3D) array receiving L reflections of a narrowband far-field signal $s(t)$ with TDs $\tau_1, \cdots, \tau_L$, incident azimuth angles $\theta_1, \cdots, \theta_L$ and incident elevation angles $\phi_1, \cdots, \phi_L$. The complex snapshot of the m-th sensor at time t_n can be modeled as

$$x_m(t_n) = \sum_{l=1}^{L} \beta_l a_m(\theta_l, \phi_l) s(t_n - \tau_l) + w_m(t_n) \qquad (1)$$

for $n = 1, \cdots, N$, where β_l is a complex coefficient representing the attenuation factor (phase shift and amplitude attenuation) of the l-th reflection. The complex channel fadings are assumed to be constant within a data burst such that β_l, $l \in \{1, \cdots, L\}$, is not dependent on t. The complex signal $s(t)$ is known. $w_m(t_n)$ is zero-mean white Gaussian noise which is independent to the source signal. Let $\boldsymbol{\chi}_m \in \mathbb{R}^{3\times 1}$ denote the 3D position vector of the m-th sensor, then, the steering response of the m-th sensor toward direction (θ, ϕ) can be expressed as $a_m(\theta, \phi) = e^{-j2\pi \boldsymbol{\chi}_m^T \boldsymbol{\rho}/\lambda}$, where λ is the wavelength, $\boldsymbol{\rho} = [\cos\theta\cos\phi,\ \sin\theta\cos\phi,\ \sin\phi]^T$ is the 3D unit vector associated with (θ, ϕ), and $\boldsymbol{\chi}_m^T \boldsymbol{\rho}$ is the range difference between the signals received at the m-th sensor and the origin (reference point). In a vector form, the $M \times 1$ snapshot vector of the (discrete) array outputs can be expressed as

$$\mathbf{x}(t_n) = \sum_{l=1}^{L} \beta_l \mathbf{a}(\theta_l, \phi_l) s(t_n - \tau_l) + \mathbf{w}(t_n) \qquad (2)$$

where

$$\begin{aligned} \mathbf{x}(t_n) &= [x_1(t_n), \cdots, x_M(t_n)]^T \\ \mathbf{w}(n) &= [w_1(t_n), \cdots, w_M(t_n)]^T \\ \mathbf{a}(\theta, \phi) &= [a_1(\theta, \phi), \cdots, a_M(\theta, \phi)]^T. \end{aligned}$$

In this work, we consider the frequency-domain model as it facilitates the development of efficient ML estimator. In the frequency-domain, the signal of the m-th sensor at the k-th frequency bin (or subcarrier), $0 \leq k \leq K$, can be modeled as

$$X_m(\omega_k) = \sum_{l=1}^{L} \beta_l a_m(\theta_l, \phi_l) S(\omega_k) e^{-j\omega_k \tau_l} + W_m(\omega_k) \qquad (3)$$

where K is the number of the effective frequency bins (or subcarriers) of the signal, $X_m(\omega_k)$, $S(\omega_k)$ and $W_m(\omega_k)$ are respectively the discrete Fourier transform (DFT) of $x_m(t_n)$, $s(t_n)$ and $w_m(t_n)$. In a vector form, the array outputs in the frequency-domain can be expressed as

$$\mathbf{x}(k) = \mathbf{D}(k)\boldsymbol{\beta} + \mathbf{w}(k) \qquad (4)$$

where $\boldsymbol{\beta} = [\beta_1, \cdots, \beta_L]^T$ and

$$\begin{aligned} \mathbf{x}(k) &= [X_1(\omega_k), \cdots, X_M(\omega_k)]^T \\ \mathbf{w}(k) &= [W_1(\omega_k), \cdots, W_M(\omega_k)]^T \\ \mathbf{D}(k) &= [\mathbf{a}(\theta_1, \phi_1)e^{-j\omega_k\tau_1}, \cdots, \mathbf{a}(\theta_L, \phi_L)e^{-j\omega_k\tau_L}]S(\omega_k). \end{aligned}$$

Note that, in some applications such as in WiFi and mobile wireless communication systems, the channel state information (CSI) may be given instead of the time-domain samples. The CSI is usually obtained via a deconvolution of the known training sequence and pulse shape function. In this case, the proposed method can be directly applied via setting $S(\omega_k) = 1$ in the model (4).

B. Gaussian Maximum Likelihood Estimator

We assume the noise spectrum vector $\mathbf{w}(k)$ is zero-mean circularly complex Gaussian distributed with variance σ^2 in each element, i.e., $E\{\mathbf{w}(k)\mathbf{w}^H(k)\} = \sigma^2\mathbf{I}_M$ and $E\{\mathbf{w}(k)\mathbf{w}^T(k)\} = \mathbf{0}_M$ for $k = 0, \cdots, K$. Note that, due to the transformation to the frequency-domain and by the central limit theorem, the noise spectrum vector $\mathbf{w}(k)$ asymptotically approaches a Gaussian distribution, even when the actual time-domain noise follows an arbitrary (independent and identically distributed) distribution (with bounded variance) other than Gaussian. In this sense, in some practical cases, the frequency-domain model may be more favorable than the time-domain model, as the noise model in the former is more reliable than

This article has been accepted for publication in a future issue of this journal, but has not been fully edited. Content may change prior to final publication. Citation information: DOI 10.1109/TVT.2018.2794322, IEEE Transactions on Vehicular Technology

that in the latter. Let $\boldsymbol{\theta} = [\theta_1, \cdots, \theta_L]^T$, $\boldsymbol{\phi} = [\phi_1, \cdots, \phi_L]^T$, $\boldsymbol{\tau} = [\tau_1, \cdots, \tau_L]^T$ and

$$\boldsymbol{\Omega} = [\boldsymbol{\theta}^T, \boldsymbol{\phi}^T, \boldsymbol{\tau}^T, \boldsymbol{\beta}^T, \sigma^2]^T$$

which contains all the unknown parameters in the model. Then, the likelihood function of $\boldsymbol{\Omega}$ can be expressed as

$$f(\boldsymbol{\Omega}) = \frac{1}{(\pi\sigma^2)^{MN}} \exp\left\{-\frac{1}{\sigma^2}\sum_{k=1}^{K}\|\mathbf{g}(k)\|^2\right\}$$

with

$$\mathbf{g}(k) = \mathbf{x}(k) - \mathbf{D}(k)\boldsymbol{\beta}.$$

The according log-likelihood is

$$\mathcal{L}(\boldsymbol{\Omega}) = -MN\log\sigma^2 - \frac{1}{\sigma^2}\sum_{k=1}^{K}\|\mathbf{g}(k)\|^2$$

and the ML estimator for $\boldsymbol{\Omega}$ is given by

$$\hat{\boldsymbol{\Omega}} = \arg\max_{\boldsymbol{\Omega}} \mathcal{L}(\boldsymbol{\Omega}).$$

As the dependency of the log-likelihood function with respect to $\boldsymbol{\theta}$, $\boldsymbol{\phi}$, $\boldsymbol{\tau}$ and $\boldsymbol{\beta}$ is through $\|\mathbf{g}(k)\|^2$, and $\|\mathbf{g}(k)\|^2$ is independent of σ^2, the concentrated ML estimator for $\boldsymbol{\theta}$, $\boldsymbol{\phi}$, $\boldsymbol{\tau}$ and $\boldsymbol{\beta}$ is given by

$$\left(\hat{\boldsymbol{\theta}}, \hat{\boldsymbol{\phi}}, \hat{\boldsymbol{\tau}}, \hat{\boldsymbol{\beta}}\right) = \arg\min_{\boldsymbol{\theta},\boldsymbol{\phi},\boldsymbol{\tau},\boldsymbol{\beta}} \sum_{k=1}^{K}\|\mathbf{g}(k)\|^2. \tag{5}$$

Since only the TDs and DOAs are of interest, we can further concentrate the ML estimator on these blocks of parameters. Specifically, let

$$\tilde{\mathbf{x}} = [\mathbf{x}^T(1), \cdots, \mathbf{x}^T(K)]^T$$
$$\tilde{\mathbf{D}} = [\mathbf{D}^T(1), \cdots, \mathbf{D}^T(K)]^T$$

the formulation (5) can be more compactly written as

$$\left(\hat{\boldsymbol{\theta}}, \hat{\boldsymbol{\phi}}, \hat{\boldsymbol{\tau}}, \hat{\boldsymbol{\beta}}\right) = \arg\min_{\boldsymbol{\theta},\boldsymbol{\phi},\boldsymbol{\tau},\boldsymbol{\beta}} \left\|\tilde{\mathbf{x}} - \tilde{\mathbf{D}}\boldsymbol{\beta}\right\|^2. \tag{6}$$

For fixed $\boldsymbol{\theta}$, $\boldsymbol{\phi}$ and $\boldsymbol{\tau}$, minimizing (6) with respect to $\boldsymbol{\beta}$ yields

$$\hat{\boldsymbol{\beta}} = (\tilde{\mathbf{D}}^H\tilde{\mathbf{D}})^{-1}\tilde{\mathbf{D}}^H\tilde{\mathbf{x}}$$

which, when substituted into (6), yields the ML estimator for $\boldsymbol{\theta}$, $\boldsymbol{\phi}$ and $\boldsymbol{\tau}$ as

$$\left(\hat{\boldsymbol{\theta}}, \hat{\boldsymbol{\phi}}, \hat{\boldsymbol{\tau}}\right) = \arg\min_{\boldsymbol{\theta},\boldsymbol{\phi},\boldsymbol{\tau}} \left\|\mathbf{P}_{\tilde{\mathbf{D}}}^{\perp}\mathbf{x}\right\|^2 \tag{7}$$

where $\mathbf{P}_{\tilde{\mathbf{D}}}^{\perp}$ is the complement orthogonal projection defined as $\mathbf{P}_{\tilde{\mathbf{D}}}^{\perp} = \mathbf{I} - \tilde{\mathbf{D}}(\tilde{\mathbf{D}}^H\tilde{\mathbf{D}})^{-1}\tilde{\mathbf{D}}^H$.

For L multipath reflections, direct minimization of (7) involves a $3L$-dimensional searching procedure, which is prohibitive for practical applications even for a moderate value of L. In the following, we develop a more efficient iterative algorithm to approximately solve the ML formulation.

III. An Approximate Maximum Likelihood Algorithm

In this section, we propose an iterative algorithm to approximately solve the ML formulation. The iterative scheme used in this algorithm is similar to the iterative algorithms in [10], [30]. The proposed AML algorithm updates the DOA (azimuth and elevation) and TD parameters alternatingly in solving the ML formulation. Intensive numerical studies show that, with a proper initialization, the alternating procedure of the AML algorithm can achieve sufficient good performance within a few iterations.

A. Proposed AML Algorithm

Define

$$\mathbf{A}(\boldsymbol{\theta}, \boldsymbol{\phi}) = [\mathbf{a}(\theta_1, \phi_1), \cdots, \mathbf{a}(\theta_L, \phi_L)]$$
$$\mathbf{r}(k, \boldsymbol{\tau}) = [e^{-j\omega_k\tau_1}, \cdots, e^{-j\omega_k\tau_L}]^T S(\omega_k)$$

and

$$\mathbf{u}(k, \boldsymbol{\tau}) = \mathrm{diag}\{\boldsymbol{\beta}\}\mathbf{r}(k, \boldsymbol{\tau}) \tag{8}$$
$$\mathbf{B} = \mathbf{A}(\boldsymbol{\theta}, \boldsymbol{\phi})\mathrm{diag}\{\boldsymbol{\beta}\}. \tag{9}$$

First, we derive an estimator for $\boldsymbol{\theta}$, $\boldsymbol{\phi}$ and $\boldsymbol{\beta}$ conditioned on $\boldsymbol{\tau}$. Specifically, given an estimation of $\boldsymbol{\tau}$, denoted by $\hat{\boldsymbol{\tau}}$, the minimization problem (5) can be rewritten as

$$\left(\hat{\boldsymbol{\theta}}, \hat{\boldsymbol{\phi}}, \hat{\boldsymbol{\beta}}\right) = \arg\min_{\boldsymbol{\theta},\boldsymbol{\phi},\boldsymbol{\beta}} \sum_{k=1}^{K}\|\mathbf{x}(k) - \mathbf{B}\mathbf{r}(k, \hat{\boldsymbol{\tau}})\|^2. \tag{10}$$

Instead of minimizing (10) directly with respect to $\boldsymbol{\theta}$, $\boldsymbol{\phi}$ and $\boldsymbol{\beta}$, we minimize it first with respect to the unstructured matrix $\mathbf{B}$, for which the explicit solution is given by

$$\hat{\mathbf{B}} = \left[\sum_{k=1}^{K}\mathbf{x}(k)\mathbf{r}^H(k, \hat{\boldsymbol{\tau}})\right]\left[\sum_{k=1}^{K}\mathbf{r}(k, \hat{\boldsymbol{\tau}})\mathbf{r}^H(k, \hat{\boldsymbol{\tau}})\right]^{-1}. \tag{11}$$

Let $\hat{\mathbf{b}}_l$ denote the l-th column of $\hat{\mathbf{B}}$, i.e., $\hat{\mathbf{B}} = [\hat{\mathbf{b}}_1, \cdots, \hat{\mathbf{b}}_L]$. From (9), only the l-th column of $\mathbf{B}$ is dependent on θ_l, ϕ_l and β_l. Thus, given an estimation $\hat{\mathbf{B}}$, we can estimate θ_l, ϕ_l and β_l via the following formulation

$$\left(\hat{\theta}_l, \hat{\phi}_l, \hat{\beta}_l\right) = \arg\min_{\theta,\phi,\beta} \left\|\hat{\mathbf{b}}_l - \beta\mathbf{a}(\theta, \phi)\right\|^2. \tag{12}$$

for $l = 1, \cdots, L$. The solution to (12) is given by

$$\left(\hat{\theta}_l, \hat{\phi}_l\right) = \arg\max_{\theta,\phi} \frac{\|\hat{\mathbf{b}}_l^H\mathbf{a}(\theta, \phi)\|^2}{\|\mathbf{a}(\theta, \phi)\|^2} \tag{13}$$

and

$$\hat{\beta}_l = \frac{\mathbf{a}^H(\hat{\theta}_l, \hat{\phi}_l)\hat{\mathbf{b}}_l}{\|\mathbf{a}(\hat{\theta}_l, \hat{\phi}_l)\|^2}. \tag{14}$$

Next, we estimate $\boldsymbol{\tau}$ and $\boldsymbol{\beta}$ conditioned on $\boldsymbol{\theta}$ and $\boldsymbol{\phi}$. Specifically, given an estimation of $\boldsymbol{\theta}$ and $\boldsymbol{\phi}$, denoted by $\hat{\boldsymbol{\theta}}$ and $\hat{\boldsymbol{\phi}}$, the minimization problem (5) can be rewritten as

$$\left(\hat{\boldsymbol{\tau}}, \hat{\boldsymbol{\beta}}\right) = \arg\min_{\boldsymbol{\tau},\boldsymbol{\beta}} \sum_{k=1}^{K}\left\|\mathbf{x}(k) - \mathbf{A}(\hat{\boldsymbol{\theta}}, \hat{\boldsymbol{\phi}})\mathbf{u}(k, \boldsymbol{\tau})\right\|^2. \tag{15}$$

In a similar manner to (10), we do not minimize (15) directly with respect to $\boldsymbol{\tau}$ and $\boldsymbol{\beta}$ rather than minimize it first with respect to the unstructured vectors $\mathbf{u}(k, \boldsymbol{\tau})$ for $k = 1, \cdots, K$,

This article has been accepted for publication in a future issue of this journal, but has not been fully edited. Content may change prior to final publication. Citation information: DOI 10.1109/TVT.2018.2794322, IEEE Transactions on Vehicular Technology

which yields the following explicit solution

$$\hat{\mathbf{u}}(k,\boldsymbol{\tau}) = \left[\mathbf{A}^H(\hat{\boldsymbol{\theta}},\hat{\boldsymbol{\phi}})\mathbf{A}(\hat{\boldsymbol{\theta}},\hat{\boldsymbol{\phi}})\right]^{-1}\mathbf{A}^H(\hat{\boldsymbol{\theta}},\hat{\boldsymbol{\phi}})\mathbf{x}(k). \quad (16)$$

Define

$$\hat{\mathbf{V}} = [\hat{\mathbf{v}}_1,\cdots,\hat{\mathbf{v}}_L] = \begin{bmatrix} \hat{\mathbf{u}}^T(1,\boldsymbol{\tau})/S(\omega_1) \\ \vdots \\ \hat{\mathbf{u}}^T(K,\boldsymbol{\tau})/S(\omega_K) \end{bmatrix}.$$

From (8), the dependency of $\mathbf{u}(k,\boldsymbol{\tau})$ with respect to τ_l and β_l is only through the l-th element of $\mathbf{u}(k,\boldsymbol{\tau})$. Thus, given an estimation $[\hat{\mathbf{v}}_1,\cdots,\hat{\mathbf{v}}_L]$, we can estimate τ_l and β_l via the following formulation

$$\left(\hat{\tau}_l,\hat{\beta}_l\right) = \arg\min_{\tau,\beta}\|\hat{\mathbf{v}}_l - \beta\mathbf{t}(\tau)\|^2 \quad (17)$$

for $l=1,\cdots,L$, where $\mathbf{t}(\tau)=[e^{-j\omega_1\tau},\cdots,e^{-j\omega_K\tau}]^T$. The solution to (17) is given by

$$\hat{\tau}_l = \arg\max_{\tau}\left\|\mathbf{t}^H(\tau)\hat{\mathbf{v}}_l\right\|^2 \quad (18)$$

and

$$\hat{\beta}_l = \frac{1}{N}\mathbf{t}^H(\hat{\tau}_l)\hat{\mathbf{v}}_l. \quad (19)$$

Since the ML formulation is nonconvex, the performance of the ML estimator is closely related to the initialization. In the following, we give an initialization scheme for the azimuth and elevation angles which follows similarly to [31]. Specifically, given the estimated parameters of the first $(l-1)$ multipath signals, denoted by $(l-1)$-dimensional vectors $\hat{\boldsymbol{\theta}}^{(l-1)}$, $\hat{\boldsymbol{\phi}}^{(l-1)}$, $\hat{\boldsymbol{\tau}}^{(l-1)}$ and $\hat{\boldsymbol{\beta}}^{(l-1)}$, the azimuth and elevation angles of the l-th multipath signal are estimated as

$$\left(\hat{\theta}_l,\hat{\phi}_l\right) = \arg\max_{\theta,\phi}\mathbf{a}^H(\theta,\phi)\mathbf{R}_x^{(l)}\mathbf{a}(\theta,\phi) \quad (20)$$

where

$$\mathbf{R}_x^{(l)} = \frac{1}{N}\sum_{n=1}^{N}\mathbf{x}^{(l)}(t_n)\left(\mathbf{x}^{(l)}(t_n)\right)^H$$

with

$$\mathbf{x}^{(l)}(t_n) = \mathbf{x}(t_n) - \sum_{i=1}^{l-1}\hat{\beta}_i^{(l-1)}\mathbf{a}(\hat{\theta}_i^{(l-1)},\hat{\phi}_i^{(l-1)})s(t_n-\hat{\tau}_i^{(l-1)}).$$

In fact, $\mathbf{R}_x^{(l)}$ is the covariance matrix of the residual after subtracting the contributions of the first $(l-1)$ multipath signals using the estimated parameters. If only the CSI is given such as in WiFi, i.e., given the frequency data (4) with $S(\omega_k)=1$, we can obtain an initialization for the azimuth and elevation of the l-th multipath signal in a similar manner via solving (20) with the use of

$$\mathbf{R}_x^{(l)} = \frac{1}{K}\sum_{k=1}^{K}\mathbf{x}^{(l)}(k)\left(\mathbf{x}^{(l)}(k)\right)^H$$

which is covariance matrix of the residual computed in the frequency-domain with

$$\mathbf{x}^{(l)}(k) = \mathbf{x}(k) - \sum_{i=1}^{l-1}\hat{\beta}_i^{(l-1)}\mathbf{a}(\hat{\theta}_i^{(l-1)},\hat{\varphi}_i^{(l-1)})e^{-j\omega_k\hat{\tau}_i^{(l-1)}}.$$

The proposed AML algorithm is summarized as follows. As will be shown in Section V, this new algorithm can achieve satisfactory performance in only a few iterations.

AML Algorithm

For: $l=1,\cdots,L$
  Estimate θ_l and ϕ_l using (20) to obtain an initialization for $\boldsymbol{\theta}^{(l)}$ and $\boldsymbol{\phi}^{(l)}$.
  While not converged **do**
    1) Estimate the TDs via (16) and (18), to obtain $\hat{\boldsymbol{\tau}}^{(l)}$.
    2) Estimate the unstructured matrix $\mathbf{B}$ via (11) using the so-obtained $\hat{\boldsymbol{\tau}}^{(l)}$.
    3) Using $\hat{\mathbf{B}}$, estimate the azimuth angle $\boldsymbol{\theta}^{(l)}$ and elevation angle $\boldsymbol{\phi}^{(l)}$ via (13).
  End while
End for
Output: $\hat{\boldsymbol{\theta}}$, $\hat{\boldsymbol{\phi}}$, $\hat{\boldsymbol{\tau}}$

The computational complexity of (16) is $O(K(L^3+ML^2+M^2L+L^2))$, while that of (18) is $O(KLN_t)$ with N_t be the grid number in the time delay domain. In (11), it involves the matrix inverse and matrix multiplication, the computational complexity is $O(KML+KL^2+ML^2+L^3)$. In (13), the computational complexity is $O(MLN_d)$, where N_d is the grid number in the DOA domain. The total computational complexity in each iteration is $O(K(L^3+ML^2+M^2L+L^2)+KML+ML^2+L^3+KLN_t+MLN_d)$.

B. Efficient Implementation of the AML Algorithm

In the above AML algorithm, a 2D search is required in estimating the azimuth and elevation via (13), which is the dominant computational complexity in each iteration. Since the subproblem (13) is only dependent on the azimuth and elevation parameters of a single path, we can estimate them in an alternative manner. For example, given the latest estimated elevation of the l-th path, denoted by $\hat{\phi}_l$, we first estimate θ_l with fixed $\hat{\phi}_l$ to obtain $\hat{\theta}_l$, then, we obtain a refined estimate of ϕ_l with fixed $\hat{\theta}_l$. This procedure is repeated until converged, which often converges within a few iterations. In such a manner, the 2D search in (13) is replaced by multiple 1D searches.

Moreover, a warm-start strategy can be used to further considerably reduce the computational burden of this iterative algorithm. Specifically, in solving (13), we can restrict the searching range of θ_l and ϕ_l based on their latest estimates or initialization, i.e., using a properly small searching range for these two parameters around their latest estimated values given by the latest iteration or initialization. This strategy can also be used in estimating the TDs via (18).

Furthermore, to efficiently obtain an initialization by (20), we can use a relative large searching step, since a coarse-grained initialization is enough for the AML algorithm to achieve satisfactory performance. For example, in the simulations in Section V, we use a searching step $\Delta\theta{=}\Delta\phi{=}\,10^{\circ}$ in solving (20). In this case, for a typical searching range $0^{\circ}\le\theta_l<360^{\circ}$ and $0^{\circ}\le\phi_l\le 90^{\circ}$, there are only 324 (36×9) grids in the 2D searching space.

This article has been accepted for publication in a future issue of this journal, but has not been fully edited. Content may change prior to final publication. Citation information: DOI 10.1109/TVT.2018.2794322, IEEE Transactions on Vehicular Technology

IV. Cramer-Rao Bound and Analysis

This section provides explicit expression of the CRB for joint DOA and TD estimation, based on which we give some analysis on the advantage of joint DOA and TD estimation over DOA-only estimation. These theoretical analyses are new in the literature studying joint DOA and TD estimation. Although the advantage of joint estimation over DOA-only estimation has been empirically shown long ago, e.g., in [10], to the best of our knowledge, the following analysis (see Result 2) is the first theoretical proof of this advantage.

A. Cramer-Rao Bound

1) CRB for joint DOA and TD estimation

Denote $\boldsymbol{\Theta} = [\boldsymbol{\theta}^T, \boldsymbol{\phi}^T]^T$, $\tilde{\boldsymbol{\beta}} = [\boldsymbol{\beta}^T, \boldsymbol{\beta}^T]^T$, $\mathbf{D}(k) = S(\omega_k)\left[\mathbf{d}_k(\theta_1,\phi_1,\tau_1),\cdots,\mathbf{d}_k(\theta_L,\phi_L,\tau_L)\right]$ with $\mathbf{d}_k(\theta,\phi,\tau) = \mathbf{a}(\theta,\phi)e^{-j\omega_k\tau}$, and

$$\boldsymbol{\Gamma}_1 = \Re\left\{\left(\tilde{\mathbf{E}}^H\mathbf{P}_{\tilde{\mathbf{D}}}^{\perp}\tilde{\mathbf{E}}\right)\odot\left(\tilde{\boldsymbol{\beta}}^*\tilde{\boldsymbol{\beta}}^T\right)\right\}$$
$$\boldsymbol{\Gamma}_2 = \Re\left\{\left(\tilde{\mathbf{E}}^H\mathbf{P}_{\tilde{\mathbf{D}}}^{\perp}\tilde{\boldsymbol{\Lambda}}\right)\odot\left(\tilde{\boldsymbol{\beta}}^*\boldsymbol{\beta}^T\right)\right\}$$
$$\boldsymbol{\Gamma}_3 = \Re\left\{\left(\tilde{\boldsymbol{\Lambda}}^H\mathbf{P}_{\tilde{\mathbf{D}}}^{\perp}\tilde{\boldsymbol{\Lambda}}\right)\odot\left(\boldsymbol{\beta}^*\boldsymbol{\beta}^T\right)\right\}$$

where $\mathbf{P}_{\tilde{\mathbf{D}}}^{\perp} = \mathbf{I}_{MK} - \tilde{\mathbf{D}}(\tilde{\mathbf{D}}^H\tilde{\mathbf{D}})^{-1}\tilde{\mathbf{D}}^H$, $\tilde{\mathbf{E}} = [\mathbf{E}^T(1),\cdots,\mathbf{E}^T(K)]^T$, $\tilde{\boldsymbol{\Lambda}} = [\boldsymbol{\Lambda}^T(1),\cdots,\boldsymbol{\Lambda}^T(K)]^T$, and $\tilde{\mathbf{D}} = [\mathbf{D}^T(1),\cdots,\mathbf{D}^T(K)]^T$ with

$$\mathbf{E}(k) = S(\omega_k)\left[\frac{\partial\mathbf{d}_k(\theta_1,\phi_1,\tau_1)}{\partial\theta_1},\cdots,\frac{\partial\mathbf{d}_k(\theta_L,\phi_L,\tau_L)}{\partial\theta_L},\right.$$
$$\left.\frac{\partial\mathbf{d}_k(\theta_1,\phi_1,\tau_1)}{\partial\phi_1},\cdots,\frac{\partial\mathbf{d}_k(\theta_L,\phi_L,\tau_L)}{\partial\phi_L}\right]$$

$$\boldsymbol{\Lambda}(k) = S(\omega_k)\left[\frac{\partial\mathbf{d}_k(\theta_1,\phi_1,\tau_1)}{\partial\tau_1},\cdots,\frac{\partial\mathbf{d}_k(\theta_L,\phi_L,\tau_L)}{\partial\tau_L}\right].$$

The CRB formulae for the DOA and TD are given as follows (derived in Appendix A).

Result 1: The $2L\times 2L$ deterministic CRB matrix for the azimuth and elevation DOAs is given by

$$\mathbf{CRB}_{\boldsymbol{\Theta\Theta}}^{\mathrm{J}} = \frac{\sigma^2}{2}\left(\boldsymbol{\Gamma}_1 - \boldsymbol{\Gamma}_2\boldsymbol{\Gamma}_3^{-1}\boldsymbol{\Gamma}_2^T\right)^{-1} \tag{21}$$

and the $L\times L$ deterministic CRB matrix for the TDs is given by

$$\mathbf{CRB}_{\boldsymbol{\tau\tau}}^{\mathrm{J}} = \frac{\sigma^2}{2}\left(\boldsymbol{\Gamma}_3 - \boldsymbol{\Gamma}_2^T\boldsymbol{\Gamma}_1^{-1}\boldsymbol{\Gamma}_2\right)^{-1}. \tag{22}$$

2) CRB for DOA-only estimation

Rewrite the model (4) as

$$\mathbf{x}(k) = \mathbf{A}(\boldsymbol{\theta},\boldsymbol{\phi})\mathbf{c}(k) + \mathbf{w}(k) \tag{23}$$

where $\mathbf{c}(k) = [\beta_1 e^{-j\omega_k\tau_1}S(\omega_k),\ \cdots,\ \beta_L e^{-j\omega_k\tau_L}S(\omega_k)]^T$. Then, treating $\mathbf{c}(k)$ as the unknown source signals, we can estimate the DOA (azimuth and elevation) using a traditional DOA-only estimator without the consideration of the TD. In this case, the deterministic CRB for DOA-only estimation is given by [32], [36]

$$\mathbf{CRB}_{\boldsymbol{\Theta\Theta}}^{\mathrm{O}} = \frac{\sigma^2}{2K}\left[\Re\left\{\left(\boldsymbol{\Psi}^H\mathbf{P}_{\mathbf{A}}^{\perp}\boldsymbol{\Psi}\right)\odot\mathbf{R}_{\tilde{\mathbf{c}}}\right\}\right]^{-1} \tag{24}$$

where $\tilde{\mathbf{c}}(k) = [\mathbf{c}^T(k),\ \mathbf{c}^T(k)]^T$, $\mathbf{P}_{\mathbf{A}}^{\perp} = \mathbf{I}_M - \mathbf{P}_{\mathbf{A}} = \mathbf{I}_M - \mathbf{A}(\mathbf{A}^H\mathbf{A})^{-1}\mathbf{A}$, and

$$\mathbf{R}_{\tilde{\mathbf{c}}} = \frac{1}{K}\sum_{k=1}^{K}\tilde{\mathbf{c}}^*(k)\tilde{\mathbf{c}}^T(k)$$

$$\boldsymbol{\Psi} = \left[\frac{\partial\mathbf{a}(\theta_1,\phi_1)}{\partial\theta_1},\cdots,\frac{\partial\mathbf{a}(\theta_L,\phi_L)}{\partial\theta_L},\frac{\partial\mathbf{a}(\theta_1,\phi_1)}{\partial\phi_1},\cdots,\frac{\partial\mathbf{a}(\theta_L,\phi_L)}{\partial\phi_L}\right].$$

Note that, the signal models for the two CRBs (21) and (24) are different. In the former the single source signal is known and the multipath attenuation factors are unknown, while in the latter all the multipath incident signals are treated as unknown signals.

B. Analysis

Intuitively, since joint DOA and TD estimation simultaneously exploits the DOA and TD structure of the multipath channels, the corresponding CRB (21) should be lower than or at least equal to the CRB (24) for DOA-only estimation. This is theoretically verified by the following results.

Result 2: The DOA-related block of CRB for joint DOA and TD estimation is bounded by the associated CRB for DOA-only estimation

$$\mathbf{CRB}_{\boldsymbol{\Theta\Theta}}^{\mathrm{J}} \le \mathbf{CRB}_{\boldsymbol{\Theta\Theta}}^{\mathrm{O}}. \tag{25}$$

Proof: See Appendix B. This result is derived for joint azimuth, elevation and TD estimation, which can be directly extended to the simplified case of joint azimuth and TD estimation.

Next, we show that under some special conditions the equality in (25) is true, i.e., $\mathbf{CRB}_{\boldsymbol{\Theta\Theta}}^{\mathrm{J}} = \mathbf{CRB}_{\boldsymbol{\Theta\Theta}}^{\mathrm{O}}$.

Result 3: If all the multipath signals have the same TD, i.e., $\tau_1 = \cdots = \tau_L$, then, the DOA-related block of CRB for joint DOA and TD estimation is equivalent to that for DOA-only estimation as

$$\mathbf{CRB}_{\boldsymbol{\Theta\Theta}}^{\mathrm{J}} = \mathbf{CRB}_{\boldsymbol{\Theta\Theta}}^{\mathrm{O}} = \frac{\sigma^2}{2\sum_{k=1}^{K}|S(\omega_k)|^2}\left[\Re\left\{\left(\boldsymbol{\Psi}^H\mathbf{P}_{\mathbf{A}}^{\perp}\boldsymbol{\Psi}\right)\odot\left(\tilde{\boldsymbol{\beta}}^*\tilde{\boldsymbol{\beta}}^T\right)\right\}\right]^{-1}. \tag{26}$$

Proof: See Appendix C.

Furthermore, in the particular case of a single path, i.e., $L = 1$, we have the following result.

Result 4: In the case of $L = 1$, the CRB (21) for joint DOA and TD estimation reduces to the CRB (24) for DOA-only estimation, and the 2×2 deterministic CRB matrix for the azimuth and elevation DOAs ($\boldsymbol{\Theta} = [\theta_1,\ \phi_1]^T$) is given by

$$\mathbf{CRB}_{\boldsymbol{\Theta\Theta}}^{\mathrm{J}} = \mathbf{CRB}_{\boldsymbol{\Theta\Theta}}^{\mathrm{O}} = \frac{\sigma^2}{2|\beta_1|^2\sum_{k=1}^{K}|S(\omega_k)|^2} \times \Re\left\{\begin{bmatrix}\mathbf{a}'^H_{\theta_1}\mathbf{P}_{\mathbf{a}}^{\perp}\mathbf{a}'_{\theta_1} & \mathbf{a}'^H_{\theta_1}\mathbf{P}_{\mathbf{a}}^{\perp}\mathbf{a}'_{\phi_1}\\ \mathbf{a}'^H_{\phi_1}\mathbf{P}_{\mathbf{a}}^{\perp}\mathbf{a}'_{\theta_1} & \mathbf{a}'^H_{\phi_1}\mathbf{P}_{\mathbf{a}}^{\perp}\mathbf{a}'_{\phi_1}\end{bmatrix}^{-1}\right\} \tag{27}$$

where $\mathbf{a}'_{\theta_1} = \partial\mathbf{a}^H(\theta_1,\phi_1)/\partial\theta_1$, $\mathbf{a}'_{\phi_1} = \partial\mathbf{a}^H(\theta_1,\phi_1)/\partial\phi_1$,

This article has been accepted for publication in a future issue of this journal, but has not been fully edited. Content may change prior to final publication. Citation information: DOI 10.1109/TVT.2018.2794322, IEEE Transactions on Vehicular Technology

and $\mathbf{P}_{\mathbf{a}}^{\perp} = \mathbf{I}_M - \mathbf{a}(\theta_1,\phi_1)\mathbf{a}^H(\theta_1,\phi_1)/\|\mathbf{a}(\theta_1,\phi_1)\|^2$. Meanwhile, the deterministic CRB for τ_1 is given by

$$\mathbf{CRB}^{\mathrm{J}}_{\tau_1\tau_1} = \frac{\sigma^2 \sum_{k=1}^{K} |S(\omega_k)|^2}{2|\beta_1|^2\|\mathbf{a}(\theta_1,\phi_1)\|^2 \sum_{k=1}^{K}\sum_{n=1}^{K} \omega_k(\omega_k-\omega_n)|S(\omega_k)|^2|S(\omega_n)|^2}. \tag{28}$$

The derivation of (27) and (28) is straightforward via using $\mathbf{D}(k) = S(\omega_k)\mathbf{d}_k(\theta_1,\phi_1,\tau_1)$, $\mathbf{E}(k) = S(\omega_k)[\partial\mathbf{d}_k^T/\partial\theta_1,\ \partial\mathbf{d}_k^T/\partial\phi_1]^T$, and $\mathbf{\Lambda}(k) = -j\omega_k S(\omega_k)\mathbf{a}(\theta_1,\phi_1)e^{-j\omega_k\tau_1}$ in the single path case.

It follows from Result 3 and 4 that, in the condition that all the incident signals have the same TD as $\tau_1 = \cdots = \tau_L$ or there exists only a single path $L = 1$, $\mathbf{CRB}^{\mathrm{J}}_{\boldsymbol{\Theta\Theta}}$ is independent on the TD and $\mathbf{CRB}^{\mathrm{J}}_{\boldsymbol{\Theta\Theta}} = \mathbf{CRB}^{\mathrm{O}}_{\boldsymbol{\Theta\Theta}}$ holds. Moreover, in the single path case, the CRB (28) for TD is independent on the DOA, and it is dependent on the signal bandwidth, sensor number, and signal power, which accords well with the well-established results for TD estimation [33]–[35]. The above results imply that, the expected benefit due to joint DOA and TD estimation mainly happens in the condition that there exist multiple reflections, i.e., $L > 1$, and the TDs of the multiple reflections are well separated. In practical indoor localization scenarios, since it is often the case that $L > 1$ and the line-of-sight (LOS) signal has a smaller value than that of the multipath signals, the LOS signal can be separated from the multipath signals in the TD space by joint DOA and TD estimation if the signal bandwidth is wide enough. In this sense, joint DOA and TD estimation can effectively suppress the effect of multipath on localization accuracy.

In the following, we compare the ill-conditions of the CRB for joint DOA and TD estimation and that for DOA-only estimation to further shed some light on the benefit of joint estimation.

Assumption 1: Suppose that $L \le L_{\max}$ where $L_{\max}$ is the greatest number of the incident signals for which the parameters $\boldsymbol{\theta}$ and $\boldsymbol{\phi}$ are identifiable in the sense: for any $i,j \in \{1,\cdots,L\}$, $\mathbf{a}(\theta_i,\phi_i) = \mathbf{a}(\theta_j,\phi_j)$ if and only if $\theta_i = \theta_j$ and $\phi_i = \phi_j$.

Assumption 2: None of the elements in $\boldsymbol{\beta}$ is zero, i.e., the attenuation factor of each reflection is nonzero. Further, let $\tilde{\mathbf{d}}(\theta,\phi,\tau) = \left[S(\omega_1)\mathbf{d}_1^T(\theta,\phi,\tau),\cdots,S(\omega_N)\mathbf{d}_N^T(\theta,\phi,\tau)\right]^T$, the source signal is not a single-tone signal and for any $i,j \in \{1,\cdots,L\}$, $\tilde{\mathbf{d}}(\theta_i,\phi_i,\tau_i) = \tilde{\mathbf{d}}(\theta_j,\phi_j,\tau_j)$ if and only if $\theta_i = \theta_j$, $\phi_i = \phi_j$ and $\tau_i = \tau_j$.

Assumption 1 describes an identifiability condition of the array. Assumption 2 describes nondegenerate conditions for the considered joint DOA and TD estimation problem. For example, when the source signal is a single-tone signal, there is an ambiguity problem in estimating the TDs since the equality $\tilde{\mathbf{d}}(\theta_i,\phi_i,\tau_i) = \tilde{\mathbf{d}}(\theta_i,\phi_i,\tau_j)$ can hold for some $\tau_i \ne \tau_j$ due to the periodicity of a single-tone signal.

Result 5: Under Assumption 1 and 2, when there exist two or more multipath signals overlapped in both azimuth and elevation, the CRB for DOA-only estimation is unbounded (i.e., $\mathbf{CRB}^{\mathrm{O}}_{\boldsymbol{\Theta\Theta}} = \infty$), while the CRBs for joint DOA and TD estimation are bounded (i.e. $\mathbf{CRB}^{\mathrm{J}}_{\boldsymbol{\Theta\Theta}} < \infty$ and $\mathbf{CRB}^{\mathrm{J}}_{\boldsymbol{\tau\tau}} < \infty$) if the DOA overlapped signals have different TDs. Further, $\mathbf{CRB}^{\mathrm{J}}_{\boldsymbol{\Theta\Theta}}$ and $\mathbf{CRB}^{\mathrm{J}}_{\boldsymbol{\tau\tau}}$ are unbounded only when there exist two or more multipath signals overlapped simultaneously in azimuth, elevation and TD.

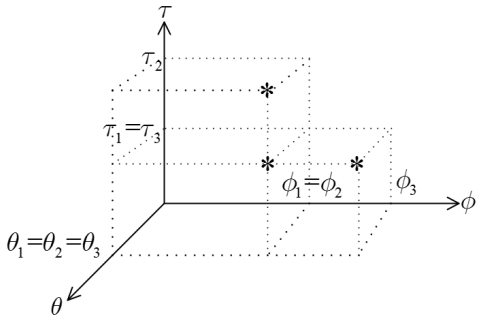

Fig. 1. Illustration of multipath signals separation in the azimuth, elevation and delay (3D) space (DOA or TD overlapped reflections can be resolved in the 3D space).

Proof: See Appendix D.

This result implies that, DOA overlapped signals (or signals with DOAs too close to be resolved by traditional DOA-only estimation) can be resolved in TD by joint DOA and TD estimation. As will be shown in the simulations, joint DOA and TD estimation improves the DOA estimation accuracy, especially for small DOA separation. Meanwhile, signals with a same TD (or with TDs too close to be resolved by TD-only estimation) can be resolved in the azimuth and/or elevation spaces. An illustration on this is given in Fig. 1, where the first and second paths which have the same azimuth and elevation can be resolved in the TD space, while the first and third paths which have the same azimuth and TD can be resolved in the elevation space.

Next, we show that, for joint DOA and TD estimation, both the CRBs for DOA and TD are dependent on the signal bandwidth.

Result 6: Let $\mathbf{CRB}^{\mathrm{J}}_{\boldsymbol{\Theta\Theta}}(K)$ and $\mathbf{CRB}^{\mathrm{J}}_{\boldsymbol{\tau\tau}}(K)$ denote the CRBs for a frequency bin (or subcarrier) number of K, then, the CRBs (21) and (22) satisfy the following relations

$$\mathbf{CRB}^{\mathrm{J}}_{\boldsymbol{\Theta\Theta}}(K) \ge \mathbf{CRB}^{\mathrm{J}}_{\boldsymbol{\Theta\Theta}}(K+1)$$
$$\mathbf{CRB}^{\mathrm{J}}_{\boldsymbol{\tau\tau}}(K) \ge \mathbf{CRB}^{\mathrm{J}}_{\boldsymbol{\tau\tau}}(K+1).$$

Proof: See Appendix E.

Moreover, the following result shows that, for joint DOA and TD estimation, both the CRBs for DOA and TD are dependent on the sensor number. This result is derived via straightforwardly extending Theorem 4.2 in [32] and the proof is omitted here for succinctness.

Result 7: Let $\mathbf{CRB}^{\mathrm{J}}_{\boldsymbol{\Theta\Theta}}(M)$ and $\mathbf{CRB}^{\mathrm{J}}_{\boldsymbol{\tau\tau}}(M)$ denote the CRBs for a sensor number of M, then, the CRBs (21) and (22) satisfy the following relations

$$\mathbf{CRB}^{\mathrm{J}}_{\boldsymbol{\Theta\Theta}}(M) \ge \mathbf{CRB}^{\mathrm{J}}_{\boldsymbol{\Theta\Theta}}(M+1)$$
$$\mathbf{CRB}^{\mathrm{J}}_{\boldsymbol{\tau\tau}}(M) \ge \mathbf{CRB}^{\mathrm{J}}_{\boldsymbol{\tau\tau}}(M+1).$$

This article has been accepted for publication in a future issue of this journal, but has not been fully edited. Content may change prior to final publication. Citation information: DOI 10.1109/TVT.2018.2794322, IEEE Transactions on Vehicular Technology

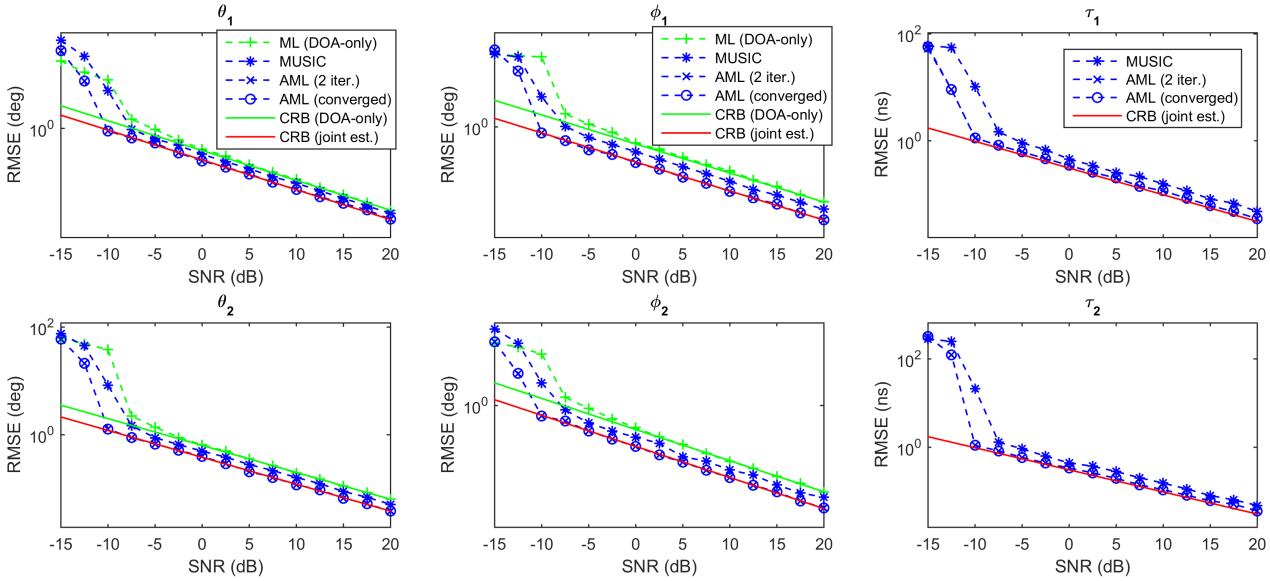

Fig. 2. RMSE of DOA and TD estimation versus SNR. Two paths with $\theta_1 = 30°$, $\theta_2 = 40°$, $\phi_1 = 50°$, $\phi_2 = 60°$, $\tau_1 = 50$ ns and $\tau_2 = 100$ ns.

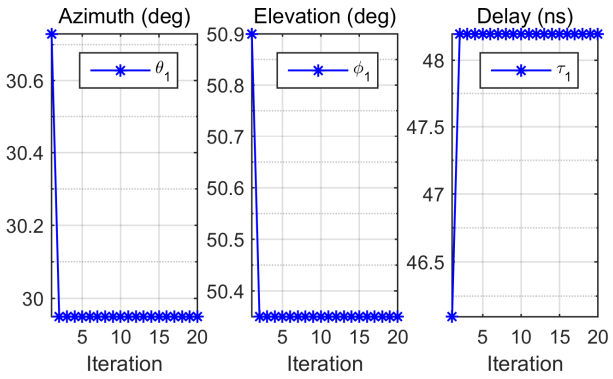

Fig. 3. Typical convergence behavior of AML with SNR = 0 dB.

V. Simulation Results

In this section, we evaluate the performance of the proposed AML algorithm and demonstrate the theoretical results via simulations. We consider a typical WiFi setting according to 802.11n, which operates in 5.32 GHz and uses 40 MHz bandwidth with 128 subcarriers and the subcarrier frequency spacing is 312.5 KHz. In practical 802.11n WiFi system, only 114 subcarriers are used for 40 MHz bandwidth. A uniform circular array (UCA) of 16 omni-directional sensors with radius $r = 1.5\lambda$ is considered. The CSI at the subcarriers are generated as (4). Mutually independent zero-mean white Gaussian noise is added to control the signal-to-noise ratio (SNR). Each provided result is an average over 500 independent runs.

In implementing the proposed AML algorithm, two cases have been considered. In the first case, each loop in the AML algorithm is terminated after 2 iterations, whilst in the second case, each loop is terminated after it is converged. The DOA-only ML estimator [31] is evaluated here for comparison, which uses the model (23) and does not take the time delay structure into consideration. The ML estimator in [31] is designed for 1D DOA estimation, we directly extended it for 2D DOA (azimuth and elevation) estimation. The MUSIC method [29] for joint azimuth, elevation and TD estimation is also evaluated here for comparison. The CRBs (21) and (22) for joint DOA and TD estimation and the CRB (24) for DOA-only estimation are plotted for comparison.

First, we consider two paths with attenuation factors $\beta_1 = e^{j\varphi_1}$ and $\beta_2 = 0.9e^{j\varphi_2}$, where the phase φ_1 and φ_2 are randomly selected from $[0,\ 2\pi]$. The DOAs of the two paths are $\theta_1 = 30°$, $\theta_2 = 40°$, $\phi_1 = 50°$, $\phi_2 = 60°$, and the time delays of the two paths are $\tau_1 = 50$ ns and $\tau_2 = 100$ ns, respectively. Fig. 2 shows the root mean square error (RMSE) of DOA and TD estimation for varying SNR. It can be seen that, the proposed AML algorithm gives significantly better performance than the DOA-only ML algorithm. It indicates that joint estimation has the potential to significantly improve the DOA estimation accuracy compared with DOA-only estimation. While the AML algorithm achieves the CRB when SNR ≥ -10 dB, the MUSIC method [29] cannot attain the CRB. Fig. 3 shows the typical convergence behavior of the proposed AML algorithm, for which only two iterations are enough for it to achieve satisfactory performance.

Fig. 4 presents the RMSE of DOA and TD estimation for varying azimuth separation $\Delta\theta$ between the two paths. The DOAs of the two paths are $\theta_1 = 30°$, $\theta_2 = \theta_1 + \Delta\theta$, $\phi_1 = 50°$, $\phi_2 = 55°$, and the time delays of the two paths are $\tau_1 = 50$ ns and $\tau_2 = 80$ ns, respectively. $\Delta\theta$ is varied from $5°$ to $30°$. The SNR is 15 dB. It can be observed that, the advantage of joint estimation over DOA-only estimation is especially conspicuous for small angular separation. When the multipaths are well separated in DOA, joint estimation and DOA-only estimation tend to give comparable performance.

Fig. 5 presents the RMSE of DOA and TD estimation for varying TD separation $\Delta\tau$ between the two paths. The DOAs of the two paths are $\theta_1 = 30°$, $\theta_2 = 40°$, $\phi_1 = 50°$, $\phi_2 = 60°$, and the time delays of the two paths are $\tau_1 = 50$

This article has been accepted for publication in a future issue of this journal, but has not been fully edited. Content may change prior to final publication. Citation information: DOI 10.1109/TVT.2018.2794322, IEEE Transactions on Vehicular Technology

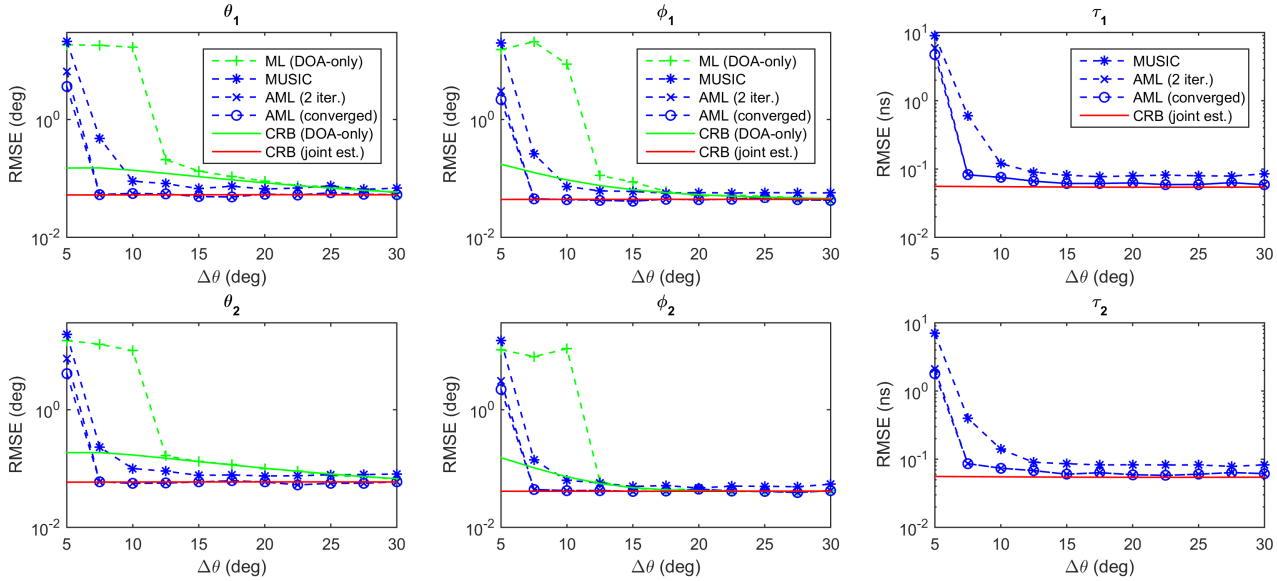

Fig. 4. RMSE of DOA and TD estimation versus azimuth separation $\Delta\theta$. Two paths with $\theta_1 = 30°$, $\theta_2 = \theta_1 + \Delta\theta$, $\phi_1 = 50°$, $\phi_2 = 55°$, $\tau_1 = 50$ ns and $\tau_2 = 80$ ns.

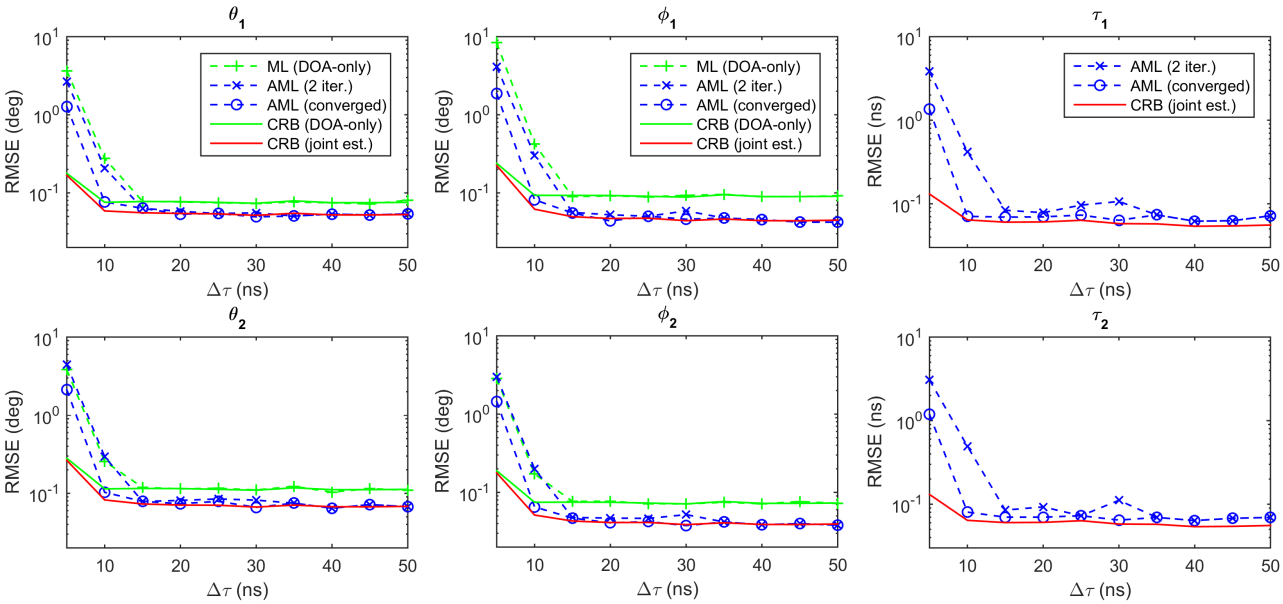

Fig. 5. RMSE of DOA and TD estimation versus TD separation $\Delta\tau$. SNR = 15 dB, two paths with $\theta_1 = 30°$, $\theta_2 = 40°$, $\phi_1 = 50°$, $\phi_2 = 60°$, $\tau_1 = 50$ ns and $\tau_2 = \tau_1 + \Delta\tau$ ns.

ns, $\tau_2 = \tau_1 + \Delta\tau$ ns, respectively. $\Delta\tau$ is varied from 5 ns to 50 ns. The SNR is 15 dB. The results in Fig. 5 indicate that, the difference between the CRBs of joint estimation and DOA-only estimation decreases as the TD separation decreases. The advantage of joint estimation over DOA-only estimation is prominent for relatively large TD separation.

The next experiment evaluates the performance dependence on the number of subcarriers. The number of subcarriers K is varied from 16 to 128, and the corresponding bandwidth is varied from 5 MHz to 40 MHz. The DOA and TD parameters of the two paths are set as same as that in Fig. 2. Fig. 6 shows the RMSE of DOA and TD estimation for varying K with SNR = 15 dB. It can be observed that, the accuracy of each compared method improves as the number of subcarriers increases, which is especially conspicuous for time delay estimation. Furthermore, the advantage of joint estimation over DOA-only estimation gets more prominent as the number of subcarriers increases.

In the last experiment, we consider the single path case, i.e., $L = 1$, with $\theta_1 = 30°$, $\phi_1 = 50°$, and $\tau_1 = 50$ ns. It can be seen from Fig. 7 that, joint estimation and DOA-only estimation give almost the same performance in the single path case. The results in Fig. 5 and Fig. 7 accord well with the theoretical results in Section IV that, the benefit due to joint DOA and TD estimation over DOA-only estimation mainly happens in the condition that there exist multiple reflections,

This article has been accepted for publication in a future issue of this journal, but has not been fully edited. Content may change prior to final publication. Citation information: DOI 10.1109/TVT.2018.2794322, IEEE Transactions on Vehicular Technology

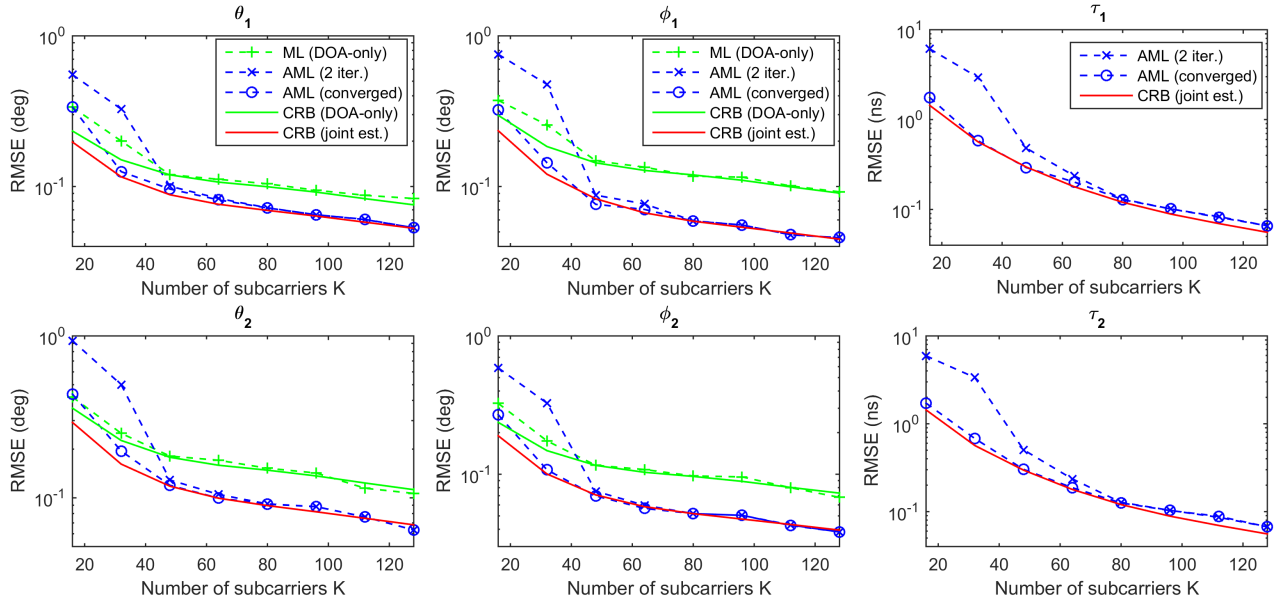

Fig. 6. RMSE of DOA and TD estimation versus subcarrier number K. SNR = 15 dB, two paths with, $\theta_1 = 30°$, $\theta_2 = 40°$, $\phi_1 = 50°$, $\phi_2 = 60°$, $\tau_1 = 50$ ns and $\tau_2 = 100$ ns.

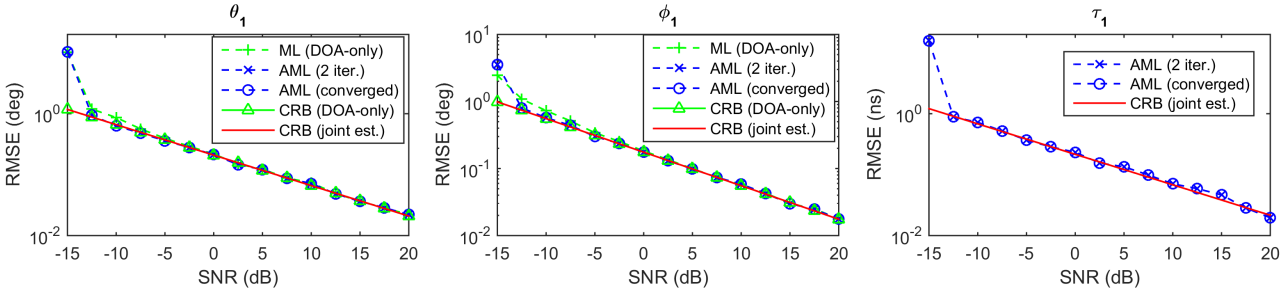

Fig. 7. RMSE of DOA and TD estimation versus SNR. A single path with $\theta_1 = 30°$, $\phi_1 = 50°$, $\tau_1 = 50$ ns.

i.e., $L > 1$, and the time delays of the multiple reflections are well separated.

VI. Conclusion

In this work, we proposed an AML algorithm for joint azimuth, elevation angles and TD estimation, which can be used for 3D indoor localization in wireless communication systems. More importantly, we analytically proved the advantage of joint DOA and TD estimation over DOA-only estimation, which is the first theoretical proof of such advantage in the literature studying joint DOA and TD estimation, although it has been empirically demonstrated long ago. The results indicate that, the benefit due to joint estimation over DOA-only estimation arises when there exist multiple reflections and the time delays of the multiple reflections are well separated. This benefit is especially conspicuous for small angular separation.

As shown in Result 5, joint estimation has the potential to resolve DOA-overlapped multipath signals in the TD space if the DOA-overlapped signals are well separated in TD. However, as shown in the simulation results, the proposed AML algorithm cannot resolve DOA-overlapped signals since the estimation (16) would break down in this condition. A future work is to develop efficient methods applicable to such condition. Moreover, this work focuses on the joint DOA and TD estimation problem and have not addressed the NLOS problem, which is an essential factor should be considered in indoor localization. We are carrying out another study specially addressing the NLOS problem in indoor localization based on spectrum fusion of multiple arrays.

Appendix A
Derivation of the CRB in Result 1

From the signal model (4) and under the assumption that the noise spectrum vector $\mathbf{w}(k)$ is zero-mean circularly complex white Gaussian distributed with variance σ^2 in each element, the Fisher information matrix (FIM) can be expressed as

$$\mathbf{F}^{\mathrm{J}} = \frac{2}{\sigma^2}\Re\left\{\frac{\partial \mathbf{b}^H}{\partial \mathbf{\Phi}}\frac{\partial \mathbf{b}}{\partial \mathbf{\Phi}^T}\right\} = \begin{bmatrix} \mathbf{F}_{\mathbf{\Theta\Theta}} & \mathbf{F}_{\mathbf{\Theta}\boldsymbol{\tau}} & \mathbf{F}_{\mathbf{\Theta}\boldsymbol{\beta}} \\ \mathbf{F}_{\boldsymbol{\tau}\mathbf{\Theta}} & \mathbf{F}_{\boldsymbol{\tau\tau}} & \mathbf{F}_{\boldsymbol{\tau}\boldsymbol{\beta}} \\ \mathbf{F}_{\boldsymbol{\beta}\mathbf{\Theta}} & \mathbf{F}_{\boldsymbol{\beta}\boldsymbol{\tau}} & \mathbf{F}_{\boldsymbol{\beta\beta}} \end{bmatrix} \quad (29)$$

where $\mathbf{\Phi} = [\mathbf{\Theta}^T, \boldsymbol{\tau}^T, \boldsymbol{\beta}_R^T, \boldsymbol{\beta}_I^T]^T \in {}^{5L\times 1}$ with $\mathbf{\Theta} = [\boldsymbol{\theta}^T, \boldsymbol{\phi}^T]^T$, $\boldsymbol{\beta}_R = \Re\{\boldsymbol{\beta}\}$, $\boldsymbol{\beta}_I = \Im\{\boldsymbol{\beta}\}$ and

$$\mathbf{b} = [\mathbf{D}^T(1), \cdots, \mathbf{D}^T(K)]^T\boldsymbol{\beta}.$$

This article has been accepted for publication in a future issue of this journal, but has not been fully edited. Content may change prior to final publication. Citation information: DOI 10.1109/TVT.2018.2794322, IEEE Transactions on Vehicular Technology

After some manipulations we have

$$\begin{aligned}
\frac{\partial \mathbf{b}^H}{\partial \boldsymbol{\Theta}} &= \mathrm{diag}\left\{[\boldsymbol{\beta}^H, \boldsymbol{\beta}^H]\right\}\left[\mathbf{E}^H(1), \cdots, \mathbf{E}^H(K)\right] \\
\frac{\partial \mathbf{b}^H}{\partial \boldsymbol{\tau}} &= \mathrm{diag}(\boldsymbol{\beta}^*)\left[\boldsymbol{\Lambda}^H(1), \cdots, \boldsymbol{\Lambda}^H(K)\right] \\
\frac{\partial \mathbf{b}^H}{\partial \boldsymbol{\beta}_R} &= \left[\mathbf{D}^H(1), \cdots, \mathbf{D}^H(K)\right] \\
\frac{\partial \mathbf{b}^H}{\partial \boldsymbol{\beta}_I} &= -j\left[\mathbf{D}^H(1), \cdots, \mathbf{D}^H(K)\right].
\end{aligned}$$

Then, we can derive the submatrices of the FIM (29) as follows

$$\mathbf{F}_{\boldsymbol{\Theta}\boldsymbol{\Theta}} = \frac{2}{\sigma^2}\Re\left\{\mathrm{diag}(\tilde{\boldsymbol{\beta}}^*)\left[\sum_{k=1}^{K}\mathbf{E}^H(k)\mathbf{E}(k)\right]\mathrm{diag}(\tilde{\boldsymbol{\beta}})\right\} \quad (30)$$

$$\mathbf{F}_{\boldsymbol{\tau}\boldsymbol{\tau}} = \frac{2}{\sigma^2}\Re\left\{\mathrm{diag}(\boldsymbol{\beta}^*)\left[\sum_{k=1}^{K}\boldsymbol{\Lambda}^H(k)\boldsymbol{\Lambda}(k)\right]\mathrm{diag}(\boldsymbol{\beta})\right\}$$

$$\mathbf{F}_{\boldsymbol{\Theta}\boldsymbol{\tau}} = \frac{2}{\sigma^2}\Re\left\{\mathrm{diag}(\tilde{\boldsymbol{\beta}}^*)\left[\sum_{k=1}^{K}\mathbf{E}^H(k)\boldsymbol{\Lambda}(k)\right]\mathrm{diag}(\boldsymbol{\beta})\right\}$$

$$\mathbf{F}_{\boldsymbol{\Theta}\boldsymbol{\beta}_R} = \frac{2}{\sigma^2}\Re\left\{\mathrm{diag}(\tilde{\boldsymbol{\beta}}^*)\sum_{k=1}^{K}\mathbf{E}^H(k)\mathbf{D}(k)\right\}$$

$$\mathbf{F}_{\boldsymbol{\Theta}\boldsymbol{\beta}_I} = -\frac{2}{\sigma^2}\Im\left\{\mathrm{diag}(\tilde{\boldsymbol{\beta}}^*)\sum_{k=1}^{K}\mathbf{E}^H(k)\mathbf{D}(k)\right\}$$

$$\mathbf{F}_{\boldsymbol{\beta}_R\boldsymbol{\beta}_R} = \frac{2}{\sigma^2}\Re\left\{\sum_{k=1}^{K}\mathbf{D}^H(k)\mathbf{D}(k)\right\}$$

$$\mathbf{F}_{\boldsymbol{\beta}_I\boldsymbol{\beta}_I} = \frac{2}{\sigma^2}\Re\left\{\sum_{k=1}^{K}\mathbf{D}^H(k)\mathbf{D}(k)\right\}$$

$$\mathbf{F}_{\boldsymbol{\beta}_R\boldsymbol{\beta}_I} = -\frac{2}{\sigma^2}\Im\left\{\sum_{k=1}^{K}\mathbf{D}^H(k)\mathbf{D}(k)\right\}$$

$$\mathbf{F}_{\boldsymbol{\tau}\boldsymbol{\beta}_R} = \frac{2}{\sigma^2}\Re\left\{\mathrm{diag}(\boldsymbol{\beta}^*)\sum_{k=1}^{K}\boldsymbol{\Lambda}^H(k)\mathbf{D}(k)\right\}$$

$$\mathbf{F}_{\boldsymbol{\tau}\boldsymbol{\beta}_I} = -\frac{2}{\sigma^2}\Im\left\{\mathrm{diag}(\boldsymbol{\beta}^*)\sum_{k=1}^{K}\boldsymbol{\Lambda}^H(k)\mathbf{D}(k)\right\}.$$

The remain submatrices of the FIM are given by

$$\begin{aligned}
\mathbf{F}_{\boldsymbol{\Theta}\boldsymbol{\beta}} &= \mathbf{F}_{\boldsymbol{\beta}\boldsymbol{\Theta}}^T = [\mathbf{F}_{\boldsymbol{\Theta}\boldsymbol{\beta}_R}, \mathbf{F}_{\boldsymbol{\Theta}\boldsymbol{\beta}_I}] \\
\mathbf{F}_{\boldsymbol{\tau}\boldsymbol{\beta}} &= \mathbf{F}_{\boldsymbol{\beta}\boldsymbol{\tau}}^T = [\mathbf{F}_{\boldsymbol{\tau}\boldsymbol{\beta}_R}, \mathbf{F}_{\boldsymbol{\tau}\boldsymbol{\beta}_I}]
\end{aligned}$$

and

$$\mathbf{F}_{\boldsymbol{\beta}\boldsymbol{\beta}} = \begin{bmatrix}\mathbf{F}_{\boldsymbol{\beta}_R\boldsymbol{\beta}_R} & \mathbf{F}_{\boldsymbol{\beta}_R\boldsymbol{\beta}_I} \\ \mathbf{F}_{\boldsymbol{\beta}_R\boldsymbol{\beta}_I} & \mathbf{F}_{\boldsymbol{\beta}_I\boldsymbol{\beta}_I}\end{bmatrix} \quad (31)$$

with $\mathbf{F}_{\boldsymbol{\beta}_I\boldsymbol{\beta}_R} = \mathbf{F}_{\boldsymbol{\beta}_R\boldsymbol{\beta}_I}^T$.

Using the partitioned matrix inversion lemma, the inverse of the CRB matrix for $\boldsymbol{\Theta}$ can be obtained as

$$\begin{aligned}
(\mathbf{CRB}_{\boldsymbol{\Theta}\boldsymbol{\Theta}}^{\mathrm{J}})^{-1} &= \mathbf{F}_{\boldsymbol{\Theta}\boldsymbol{\Theta}} - \mathbf{F}_{\boldsymbol{\Theta}\boldsymbol{\beta}}\mathbf{F}_{\boldsymbol{\beta}\boldsymbol{\beta}}^{-1}\mathbf{F}_{\boldsymbol{\Theta}\boldsymbol{\beta}}^T \\
&- \left(\mathbf{F}_{\boldsymbol{\Theta}\boldsymbol{\tau}} - \mathbf{F}_{\boldsymbol{\Theta}\boldsymbol{\beta}}\mathbf{F}_{\boldsymbol{\beta}\boldsymbol{\beta}}^{-1}\mathbf{F}_{\boldsymbol{\tau}\boldsymbol{\beta}}^T\right)\left(\mathbf{F}_{\boldsymbol{\tau}\boldsymbol{\tau}} - \mathbf{F}_{\boldsymbol{\tau}\boldsymbol{\beta}}\mathbf{F}_{\boldsymbol{\beta}\boldsymbol{\beta}}^{-1}\mathbf{F}_{\boldsymbol{\tau}\boldsymbol{\beta}}^T\right)^{-1} \\
&\times \left(\mathbf{F}_{\boldsymbol{\tau}\boldsymbol{\Theta}} - \mathbf{F}_{\boldsymbol{\tau}\boldsymbol{\beta}}\mathbf{F}_{\boldsymbol{\beta}\boldsymbol{\beta}}^{-1}\mathbf{F}_{\boldsymbol{\Theta}\boldsymbol{\beta}}^T\right). \quad (32)
\end{aligned}$$

Then, using the following rules [28]

$$\begin{bmatrix}\Re\{\mathbf{H}\} & -\Im\{\mathbf{H}\} \\ \Im\{\mathbf{H}\} & \Re\{\mathbf{H}\}\end{bmatrix}^{-1} = \begin{bmatrix}\Re\{\mathbf{H}^{-1}\} & -\Im\{\mathbf{H}^{-1}\} \\ \Im\{\mathbf{H}^{-1}\} & \Re\{\mathbf{H}^{-1}\}\end{bmatrix}$$

and

$$\begin{aligned}
\Im\{\mathbf{X}\}\Re\{\mathbf{Y}^H\} + \Re\{\mathbf{X}\}\Im\{\mathbf{Y}^H\} &= \Im\{\mathbf{X}\mathbf{Y}^H\} \\
\Re\{\mathbf{X}\}\Re\{\mathbf{Y}^H\} - \Im\{\mathbf{X}\}\Im\{\mathbf{Y}^H\} &= \Re\{\mathbf{X}\mathbf{Y}^H\}
\end{aligned}$$

the formulae in (21) is derived after straightforward manipulation. In a similar manner, the inverse of the CRB matrix for $\boldsymbol{\tau}$ is given by

$$\begin{aligned}
(\mathbf{CRB}_{\boldsymbol{\tau}\boldsymbol{\tau}}^{\mathrm{J}})^{-1} &= \mathbf{F}_{\boldsymbol{\tau}\boldsymbol{\tau}} - \mathbf{F}_{\boldsymbol{\tau}\boldsymbol{\beta}}\mathbf{F}_{\boldsymbol{\beta}\boldsymbol{\beta}}^{-1}\mathbf{F}_{\boldsymbol{\tau}\boldsymbol{\beta}}^T \\
&- \left(\mathbf{F}_{\boldsymbol{\tau}\boldsymbol{\Theta}} - \mathbf{F}_{\boldsymbol{\tau}\boldsymbol{\beta}}\mathbf{F}_{\boldsymbol{\beta}\boldsymbol{\beta}}^{-1}\mathbf{F}_{\boldsymbol{\Theta}\boldsymbol{\beta}}^T\right)\left(\mathbf{F}_{\boldsymbol{\Theta}\boldsymbol{\Theta}} - \mathbf{F}_{\boldsymbol{\Theta}\boldsymbol{\beta}}\mathbf{F}_{\boldsymbol{\beta}\boldsymbol{\beta}}^{-1}\mathbf{F}_{\boldsymbol{\Theta}\boldsymbol{\beta}}^T\right)^{-1} \\
&\times \left(\mathbf{F}_{\boldsymbol{\Theta}\boldsymbol{\tau}} - \mathbf{F}_{\boldsymbol{\Theta}\boldsymbol{\beta}}\mathbf{F}_{\boldsymbol{\beta}\boldsymbol{\beta}}^{-1}\mathbf{F}_{\boldsymbol{\tau}\boldsymbol{\beta}}^T\right)
\end{aligned}$$

and we can obtain an explicit expression as (22).

Appendix B
Proof of Result 2

First, for the DOA-only estimation case, the FIM is given by

$$\mathbf{F}^{\mathrm{O}} = \begin{bmatrix}\mathbf{F}_{\boldsymbol{\Theta}\boldsymbol{\Theta}} & \mathbf{F}_{\boldsymbol{\Theta}\mathbf{C}} \\ \mathbf{F}_{\mathbf{C}\boldsymbol{\Theta}} & \mathbf{F}_{\mathbf{C}\mathbf{C}}\end{bmatrix} \quad (33)$$

where $\mathbf{F}_{\boldsymbol{\Theta}\boldsymbol{\Theta}}$ is given by (30), $\mathbf{F}_{\boldsymbol{\Theta}\mathbf{C}} = [\mathbf{F}_{\boldsymbol{\Theta}\mathbf{c}(1)}, \cdots, \mathbf{F}_{\boldsymbol{\Theta}\mathbf{c}(K)}]$ and $\mathbf{F}_{\mathbf{C}\boldsymbol{\Theta}} = \mathbf{F}_{\boldsymbol{\Theta}\mathbf{C}}^T$ with $\mathbf{F}_{\boldsymbol{\Theta}\mathbf{c}(k)} = [\mathbf{F}_{\boldsymbol{\Theta}\mathbf{c}_R(k)}, \mathbf{F}_{\boldsymbol{\Theta}\mathbf{c}_I(k)}]$, $\mathbf{c}_R(k) = \Re\{\mathbf{c}(k)\}$, $\mathbf{c}_I(k) = \Im\{\mathbf{c}(k)\}$ and

$$\mathbf{F}_{\boldsymbol{\Theta}\mathbf{c}(k)} = \frac{2}{\sigma^2}\Re\left\{\mathrm{diag}\{\tilde{\mathbf{c}}^*(k)\}\boldsymbol{\Psi}^H\left[\mathbf{A}(\theta,\varphi),\ j\mathbf{A}(\theta,\varphi)\right]\right\}$$

$$\mathbf{F}_{\mathbf{C}\mathbf{C}} = \mathrm{blkdiag}\left\{\mathbf{F}_{\mathbf{c}(1)\mathbf{c}(1)}, \cdots, \mathbf{F}_{\mathbf{c}(K)\mathbf{c}(K)}\right\}$$

with

$$\begin{aligned}
\mathbf{F}_{\mathbf{c}(k)\mathbf{c}(k)} &= \begin{bmatrix}\mathbf{F}_{\mathbf{c}_R(k)\mathbf{c}_R(k)} & \mathbf{F}_{\mathbf{c}_R(k)\mathbf{c}_I(k)} \\ \mathbf{F}_{\mathbf{c}_I(k)\mathbf{c}_R(k)} & \mathbf{F}_{\mathbf{c}_I(k)\mathbf{c}_I(k)}\end{bmatrix} \\
&= \frac{2}{\sigma^2}\begin{bmatrix}\Re\{\mathbf{A}^H\mathbf{A}\} & -\Im\{\mathbf{A}^H\mathbf{A}\} \\ \Im\{\mathbf{A}^H\mathbf{A}\} & \Re\{\mathbf{A}^H\mathbf{A}\}\end{bmatrix}.
\end{aligned}$$

The CRB for the DOA-only estimation can be rewritten as

$$(\mathbf{CRB}_{\boldsymbol{\Theta}\boldsymbol{\Theta}}^{\mathrm{O}})^{-1} = \mathbf{F}_{\boldsymbol{\Theta}\boldsymbol{\Theta}} - \mathbf{F}_{\boldsymbol{\Theta}\mathbf{C}}\mathbf{F}_{\mathbf{C}\mathbf{C}}^{-1}\mathbf{F}_{\boldsymbol{\Theta}\mathbf{C}}^T. \quad (34)$$

From (32) and (34), to prove $\mathbf{CRB}_{\boldsymbol{\Theta}\boldsymbol{\Theta}}^{\mathrm{J}} \leq \mathbf{CRB}_{\boldsymbol{\Theta}\boldsymbol{\Theta}}^{\mathrm{O}}$, it is enough to prove that

$$\begin{aligned}
&\mathbf{F}_{\boldsymbol{\Theta}\mathbf{C}}\mathbf{F}_{\mathbf{C}\mathbf{C}}^{-1}\mathbf{F}_{\mathbf{C}\boldsymbol{\Theta}} - \mathbf{F}_{\boldsymbol{\Theta}\boldsymbol{\beta}}\mathbf{F}_{\boldsymbol{\beta}\boldsymbol{\beta}}^{-1}\mathbf{F}_{\boldsymbol{\beta}\boldsymbol{\Theta}} \\
&- \left(\mathbf{F}_{\boldsymbol{\Theta}\boldsymbol{\tau}} - \mathbf{F}_{\boldsymbol{\Theta}\boldsymbol{\beta}}\mathbf{F}_{\boldsymbol{\beta}\boldsymbol{\beta}}^{-1}\mathbf{F}_{\boldsymbol{\beta}\boldsymbol{\tau}}\right)\left(\mathbf{F}_{\boldsymbol{\tau}\boldsymbol{\tau}} - F_{\boldsymbol{\tau}\boldsymbol{\beta}}\mathbf{F}_{\boldsymbol{\beta}\boldsymbol{\beta}}^{-1}\mathbf{F}_{\boldsymbol{\beta}\boldsymbol{\tau}}\right)^{-1} \\
&\times \left(\mathbf{F}_{\boldsymbol{\tau}\boldsymbol{\Theta}} - \mathbf{F}_{\boldsymbol{\tau}\boldsymbol{\beta}}\mathbf{F}_{\boldsymbol{\beta}\boldsymbol{\beta}}^{-1}\mathbf{F}_{\boldsymbol{\beta}\boldsymbol{\Theta}}\right) \\
&\geq \mathbf{0}.
\end{aligned} \quad (35)$$

Using the standard technique of Schur complements, (35) in

This article has been accepted for publication in a future issue of this journal, but has not been fully edited. Content may change prior to final publication. Citation information: DOI 10.1109/TVT.2018.2794322, IEEE Transactions on Vehicular Technology

fact is equivalent to

$$\mathbf{M}_0 = \begin{bmatrix} \mathbf{F}_{\boldsymbol{\Theta C}}\mathbf{F}_{\mathbf{CC}}^{-1}\mathbf{F}_{\mathbf{C}\boldsymbol{\Theta}} & \mathbf{F}_{\boldsymbol{\Theta\tau}} & \mathbf{F}_{\boldsymbol{\Theta\beta}} \\ \mathbf{F}_{\boldsymbol{\tau\Theta}} & \mathbf{F}_{\boldsymbol{\tau\tau}} & \mathbf{F}_{\boldsymbol{\tau\beta}} \\ \mathbf{F}_{\boldsymbol{\beta\Theta}} & \mathbf{F}_{\boldsymbol{\beta\tau}} & \mathbf{F}_{\boldsymbol{\beta\beta}} \end{bmatrix} \geq \mathbf{0}. \tag{36}$$

In fact, it follows from the partitioned matrix inversion lemma that, the first $2L \times 2L$ block of the inverse matrix $\mathbf{M}_0^{-1}$ is equivalent to the inverse of the left term in (35). Let $\mathbf{t}(k) = [e^{-j\omega_k\tau_1}, \cdots, e^{-j\omega_k\tau_L}]^T$, $\tilde{\mathbf{t}}(k) = [\mathbf{t}^T(k),\ \mathbf{t}^T(k)]^T$, and

$$\mathbf{B}_1 = \sum_{k=1}^{K} |S(\omega_k)|^2 \mathbf{t}^*(k)\mathbf{t}^T(k)$$
$$\mathbf{B}_2 = \sum_{k=1}^{K} \omega_k |S(\omega_k)|^2 \mathbf{t}^*(k)\mathbf{t}^T(k)$$
$$\mathbf{B}_3 = \sum_{k=1}^{K} \omega_k^2 |S(\omega_k)|^2 \mathbf{t}^*(k)\mathbf{t}^T(k)$$

and using the following relations

$$\mathbf{E}^H(k)\boldsymbol{\Lambda}(k) = -j(\boldsymbol{\Psi}^H\mathbf{A}) \odot \left[\omega_k |S(\omega_k)|^2 \tilde{\mathbf{t}}^*(k)\mathbf{t}^T(k)\right]$$
$$\mathbf{E}^H(k)\mathbf{D}(k) = (\boldsymbol{\Psi}^H\mathbf{A}) \odot \left[|S(\omega_k)|^2 \tilde{\mathbf{t}}^*(k)\mathbf{t}^T(k)\right]$$
$$\boldsymbol{\Lambda}^H(k)\boldsymbol{\Lambda}(k) = (\mathbf{A}^H\mathbf{A}) \odot \left[\omega_k^2 |S(\omega_k)|^2 \mathbf{t}^*(k)\mathbf{t}(k)\right]$$
$$\mathbf{D}^H(k)\mathbf{D}(k) = (\mathbf{A}^H\mathbf{A}) \odot \left[|S(\omega_k)|^2 \mathbf{t}^*(k)\mathbf{t}^T(k)\right]$$
$$\boldsymbol{\Lambda}^H(k)\mathbf{D}(k) = j(\mathbf{A}^H\mathbf{A}) \odot \left[\omega_k |S(\omega_k)|^2 \mathbf{t}^*(k)\mathbf{t}^T(k)\right]$$

we have

$$\mathbf{F}_{\boldsymbol{\Theta C}}\mathbf{F}_{\mathbf{CC}}^{-1}\mathbf{F}_{\mathbf{C}\boldsymbol{\Theta}} = \frac{2}{\sigma^2}\Re\left\{(\boldsymbol{\Psi}^H\mathbf{P}_{\mathbf{A}}\boldsymbol{\Psi}) \odot \begin{bmatrix} \mathbf{B}_1 & \mathbf{B}_1 \\ \mathbf{B}_1 & \mathbf{B}_1 \end{bmatrix} \odot \left(\tilde{\boldsymbol{\beta}}^*\tilde{\boldsymbol{\beta}}^T\right)\right\}$$
$$\mathbf{F}_{\boldsymbol{\Theta\tau}} = \frac{2}{\sigma^2}\Re\left\{-j(\boldsymbol{\Psi}^H\mathbf{A}) \odot \begin{bmatrix} \mathbf{B}_2 \\ \mathbf{B}_2 \end{bmatrix} \odot (\tilde{\boldsymbol{\beta}}^*\boldsymbol{\beta}^T)\right\}$$
$$\mathbf{F}_{\boldsymbol{\Theta\beta}_R} = \frac{2}{\sigma^2}\Re\left\{(\boldsymbol{\Psi}^H\mathbf{A}) \odot \begin{bmatrix} \mathbf{B}_1 \\ \mathbf{B}_1 \end{bmatrix} \odot (\tilde{\boldsymbol{\beta}}^*\mathbf{1}_L^T)\right\}$$
$$\mathbf{F}_{\boldsymbol{\Theta\beta}_I} = \frac{2}{\sigma^2}\Re\left\{j(\boldsymbol{\Psi}^H\mathbf{A}) \odot \begin{bmatrix} \mathbf{B}_1 \\ \mathbf{B}_1 \end{bmatrix} \odot (\tilde{\boldsymbol{\beta}}^*\mathbf{1}_L^T)\right\}$$
$$\mathbf{F}_{\boldsymbol{\tau\tau}} = \frac{2}{\sigma^2}\Re\left\{(\mathbf{A}^H\mathbf{A}) \odot \mathbf{B}_3 \odot (\boldsymbol{\beta}^*\boldsymbol{\beta}^T)\right\}$$
$$\mathbf{F}_{\boldsymbol{\beta}_R\boldsymbol{\beta}_R} = \frac{2}{\sigma^2}\Re\left\{(\mathbf{A}^H\mathbf{A}) \odot \mathbf{B}_1\right\}$$

$$\mathbf{F}_{\boldsymbol{\beta}_I\boldsymbol{\beta}_I} = \frac{2}{\sigma^2}\Re\left\{\sum_{k=1}^{K}(\mathbf{A}^H\mathbf{A}) \odot \mathbf{B}_1\right\}$$
$$\mathbf{F}_{\boldsymbol{\beta}_R\boldsymbol{\beta}_I} = \frac{2}{\sigma^2}\Re\left\{j(\mathbf{A}^H\mathbf{A}) \odot \mathbf{B}_1\right\}$$
$$\mathbf{F}_{\boldsymbol{\tau\beta}_R} = \frac{2}{\sigma^2}\Re\left\{j(\mathbf{A}^H\mathbf{A}) \odot \mathbf{B}_2 \odot (\boldsymbol{\beta}^*\mathbf{1}_L^T)\right\}$$
$$\mathbf{F}_{\boldsymbol{\tau\beta}_I} = \frac{2}{\sigma^2}\Re\left\{-(\mathbf{A}^H\mathbf{A}) \odot \mathbf{B}_2 \odot (\boldsymbol{\beta}^*\mathbf{1}_L^T)\right\}.$$

Substituting these terms into (36), and with the use of $\mathbf{F}_{\boldsymbol{\Theta\beta}} = \mathbf{F}_{\boldsymbol{\beta\Theta}}^T = [\mathbf{F}_{\boldsymbol{\Theta\beta}_R}, \mathbf{F}_{\boldsymbol{\Theta\beta}_I}]$, $\mathbf{F}_{\boldsymbol{\tau\beta}} = \mathbf{F}_{\boldsymbol{\beta\tau}}^T = [\mathbf{F}_{\boldsymbol{\tau\beta}_R}, \mathbf{F}_{\boldsymbol{\tau\beta}_I}]$ and (31), we can express the matrix $\mathbf{M}_0$ in (36) as

$$\mathbf{M}_0 = \frac{2}{\sigma^2}\Re\left\{\mathbf{M}_1 \odot \mathbf{M}_2 \odot \mathbf{M}_3\right\} \tag{37}$$

where

$$\mathbf{M}_1 = \begin{bmatrix} \boldsymbol{\Psi}^H\mathbf{P}_{\mathbf{A}}\boldsymbol{\Psi} & -j\boldsymbol{\Psi}^H\mathbf{A} & \boldsymbol{\Psi}^H\mathbf{A} & j\boldsymbol{\Psi}^H\mathbf{A} \\ j\mathbf{A}^H\boldsymbol{\Psi} & \mathbf{A}^H\mathbf{A} & j\mathbf{A}^H\mathbf{A} & -\mathbf{A}^H\mathbf{A} \\ \mathbf{A}^H\boldsymbol{\Psi} & -j\mathbf{A}^H\mathbf{A} & \mathbf{A}^H\mathbf{A} & j\mathbf{A}^H\mathbf{A} \\ -j\mathbf{A}^H\boldsymbol{\Psi} & -\mathbf{A}^H\mathbf{A} & -j\mathbf{A}^H\mathbf{A} & \mathbf{A}^H\mathbf{A} \end{bmatrix}$$

$$\mathbf{M}_2 = \begin{bmatrix} \tilde{\mathbf{B}}_1 & \tilde{\mathbf{B}}_2 & \tilde{\mathbf{B}}_1 \\ \tilde{\mathbf{B}}_2^H & \mathbf{B}_3 & \tilde{\mathbf{B}}_2^H \\ \tilde{\mathbf{B}}_1 & \tilde{\mathbf{B}}_2 & \tilde{\mathbf{B}}_1 \end{bmatrix}$$

$$\mathbf{M}_3 = \begin{bmatrix} \tilde{\boldsymbol{\beta}}^*\tilde{\boldsymbol{\beta}}^T & \tilde{\boldsymbol{\beta}}^*\boldsymbol{\beta}^T & \tilde{\boldsymbol{\beta}}^*\mathbf{1}_{2L}^T \\ \boldsymbol{\beta}^*\tilde{\boldsymbol{\beta}}^T & \boldsymbol{\beta}^*\boldsymbol{\beta}^T & \boldsymbol{\beta}^*\mathbf{1}_{2L}^T \\ \mathbf{1}_{2L}\tilde{\boldsymbol{\beta}}^T & \mathbf{1}_{2L}\boldsymbol{\beta}^T & \mathbf{1}_{2L}\mathbf{1}_{2L}^T \end{bmatrix}$$

with

$$\tilde{\mathbf{B}}_1 = \begin{bmatrix} \mathbf{B}_1 & \mathbf{B}_1 \\ \mathbf{B}_1 & \mathbf{B}_1 \end{bmatrix}, \quad \tilde{\mathbf{B}}_2 = \begin{bmatrix} \mathbf{B}_2 \\ \mathbf{B}_2 \end{bmatrix}.$$

Then, using the fact that $\Re\{\mathbf{M}\} \geq \mathbf{0}$ if $\mathbf{M} \geq \mathbf{0}$, $\mathbf{M}_0$ is positive semidefinite if

$$\mathbf{M}_1 \odot \mathbf{M}_2 \odot \mathbf{M}_3 \geq \mathbf{0}. \tag{38}$$

From the properties of Hadamard product, (38) holds if all of $\mathbf{M}_1$, $\mathbf{M}_2$ and $\mathbf{M}_3$ are positive semidefinite. Since these three matrices can be expressed as

$$\mathbf{M}_1 = \begin{bmatrix} \boldsymbol{\Psi}^H \\ j\mathbf{A}^H \\ \mathbf{A}^H \\ -j\mathbf{A}^H \end{bmatrix} \mathbf{A}(\mathbf{A}^H\mathbf{A})^{-1}\mathbf{A}^H \begin{bmatrix} \boldsymbol{\Psi} & -j\mathbf{A} & \mathbf{A} & j\mathbf{A} \end{bmatrix}$$

$$\mathbf{M}_2 = \sum_{k=1}^{K} |S(\omega_k)|^2 \begin{bmatrix} \tilde{\mathbf{t}}^*(k) \\ \omega_k\mathbf{t}^*(k) \\ \tilde{\mathbf{t}}^*(k) \end{bmatrix} \begin{bmatrix} \tilde{\mathbf{t}}^T(k) & \omega_k\mathbf{t}^T(k) & \tilde{\mathbf{t}}^T(k) \end{bmatrix}$$

and

$$\mathbf{M}_3 = \begin{bmatrix} \tilde{\boldsymbol{\beta}}^* \\ \boldsymbol{\beta}^* \\ \mathbf{1}_{2L} \end{bmatrix} \begin{bmatrix} \tilde{\boldsymbol{\beta}}^T & \boldsymbol{\beta}^T & \mathbf{1}_{2L}^T \end{bmatrix}$$

it is easy to see that all of $\mathbf{M}_1$, $\mathbf{M}_1$ and $\mathbf{M}_3$ are positive semidefinite. Thus, (35), (36) and (38) are satisfied, which completes the proof.

APPENDIX C
PROOF OF RESULT 3

When $\tau_1 = \cdots = \tau_L$, it follows that

$$\mathbf{D}(k) = S(\omega_k)e^{-j\omega_k\tau_1}\mathbf{A}(\boldsymbol{\theta}, \boldsymbol{\phi})$$
$$\mathbf{E}(k) = S(\omega_k)e^{-j\omega_k\tau_1}\boldsymbol{\Psi}$$
$$\boldsymbol{\Lambda}(k) = -j\omega_k S(\omega_k)e^{-j\omega_k\tau_1}\mathbf{A}(\boldsymbol{\theta}, \boldsymbol{\phi})$$
$$\mathbf{c}(k) = S(\omega_k)e^{-j\omega_k\tau_1}[\beta_1, \cdots, \beta_L]^T$$

based on which we further have $\tilde{\mathbf{c}}(k) = S(\omega_k)e^{-j\omega_k\tau_1}\tilde{\boldsymbol{\beta}}$, $\tilde{\mathbf{E}}^H\mathbf{P}_{\tilde{\mathbf{D}}}^{\perp}\tilde{\boldsymbol{\Lambda}}=\mathbf{0}$, and $\tilde{\mathbf{E}}^H\mathbf{P}_{\tilde{\mathbf{D}}}^{\perp}\tilde{\mathbf{E}}=\sum_{k=1}^{K}|S(\omega_k)|^2\boldsymbol{\Psi}^H\mathbf{P}_{\mathbf{A}}^{\perp}\boldsymbol{\Psi}$, which together with (21) and (24) finally results in (26).

This article has been accepted for publication in a future issue of this journal, but has not been fully edited. Content may change prior to final publication. Citation information: DOI 10.1109/TVT.2018.2794322, IEEE Transactions on Vehicular Technology

APPENDIX D
PROOF OF RESULT 5

For the DOA-only estimation case, the FIM is given by (33). When there are $P \geq 2$ incident signals overlapped in both azimuth and elevation, that is there exists a subset $S \subset \{1, \cdots, L\}$ with size $P \geq 2$ such that $\theta_i = \theta_j$ and $\phi_i = \phi_j$ for any $i, j \in S$, it follows that $\mathbf{a}(\theta_i, \phi_i) = \mathbf{a}(\theta_j, \phi_j)$, $\partial \mathbf{a}(\theta_i, \phi_i)/\partial \theta_i = \partial \mathbf{a}(\theta_j, \phi_j)/\partial \theta_j$ and $\partial \mathbf{a}(\theta_i, \phi_i)/\partial \phi_i = \partial \mathbf{a}(\theta_j, \phi_j)/\partial \phi_j$ for any $i, j \in S$. In this case, $\mathbf{F}_{\boldsymbol{\Theta\Theta}}$ and $\mathbf{F}_{\mathbf{CC}}$ are not full-rank as $\mathrm{rank}(\mathbf{F}_{\boldsymbol{\Theta\Theta}}) \leq 2(L-P+1)$ and $\mathrm{rank}(\mathbf{F}_{\mathbf{CC}}) \leq 2K(L-P+1)$. Meanwhile, the row blocks in the FIM

$$\left[\mathbf{F}_{\mathbf{c}(k)\boldsymbol{\Theta}}, \cdots, \mathbf{0}, \cdots, \mathbf{F}_{\mathbf{c}(k)\mathbf{c}(k)}, \cdots \mathbf{0}, \cdots\right] \in \mathbb{C}^{2L \times 2(K+1)L}$$

for $k = 1, \cdots, K$, are not full-row rank. Thus, $\mathbf{CRB}^{\mathrm{O}}_{\boldsymbol{\Theta\Theta}}$ is unbounded in this case.

For the joint DOA and TD estimation case, let $\bar{\boldsymbol{\Theta}} = [\boldsymbol{\theta}^T, \boldsymbol{\phi}^T, \boldsymbol{\tau}^T]^T$, the FIM (29) can be rewritten as

$$\mathbf{F}^{\mathrm{J}} = \begin{bmatrix} \mathbf{F}_{\bar{\boldsymbol{\Theta}}\bar{\boldsymbol{\Theta}}} & \mathbf{F}_{\bar{\boldsymbol{\Theta}}\boldsymbol{\beta}} \\ \mathbf{F}_{\boldsymbol{\beta}\bar{\boldsymbol{\Theta}}} & \mathbf{F}_{\boldsymbol{\beta\beta}} \end{bmatrix}.$$

When there exists a subset $S \subset \{1, \cdots, L\}$ with size $P \geq 2$ such that $\theta_i = \theta_j$, $\phi_i = \phi_j$ and $\tau_i = \tau_j$ for any $i, j \in S$, it follows that $\tilde{\mathbf{d}}(\theta_i, \phi_i, \tau_i) = \tilde{\mathbf{d}}(\theta_j, \phi_j, \tau_j)$ for any $i, j \in S$. In this case, in a similar manner to the above discussion, it is easy to see the FIM is not full-rank and therefore $\mathbf{CRB}^{\mathrm{J}}_{\boldsymbol{\Theta\Theta}}$ and $\mathbf{CRB}^{\mathrm{J}}_{\boldsymbol{\tau\tau}}$ are unbounded. In the case that the DOA overlapped signals have different TDs, i.e., $\theta_i = \theta_j$, $\phi_i = \phi_j$ and $\tau_i \neq \tau_j$ for any $i, j \in S$, we have $\tilde{\mathbf{d}}(\theta_i, \phi_i, \tau_i) \neq \tilde{\mathbf{d}}(\theta_j, \phi_j, \tau_j)$ under Assumption 1 and 2. Then, from the decomposed expressions of the FIM in Appendix A, it is easy to see that the FIM has a full rank and $\mathbf{CRB}^{\mathrm{J}}_{\boldsymbol{\Theta\Theta}}$ and $\mathbf{CRB}^{\mathrm{J}}_{\boldsymbol{\tau\tau}}$ are bounded in this case. In other cases where there do not exist two or more multipath signals overlapped simultaneously in azimuth, elevation and TD, it also follows that $\tilde{\mathbf{d}}(\theta_i, \phi_i, \tau_i) \neq \tilde{\mathbf{d}}(\theta_j, \phi_j, \tau_j)$ for any $i, j \in \{1, \cdots, L\}$ and, thus, $\mathbf{CRB}^{\mathrm{J}}_{\boldsymbol{\Theta\Theta}}$ and $\mathbf{CRB}^{\mathrm{J}}_{\boldsymbol{\tau\tau}}$ are bounded following similar arguments.

APPENDIX E
PROOF OF RESULT 6

Let $\mathbf{F}^{\mathrm{J}}(K)$ denote the FIM (29) for a frequency bin (or subcarrier) number of K, to show $\mathbf{CRB}^{\mathrm{J}}_{\boldsymbol{\Theta\Theta}}(K) \geq \mathbf{CRB}^{\mathrm{J}}_{\boldsymbol{\Theta\Theta}}(K+1)$ and $\mathbf{CRB}^{\mathrm{J}}_{\boldsymbol{\tau\tau}}(K) \geq \mathbf{CRB}^{\mathrm{J}}_{\boldsymbol{\tau\tau}}(K+1)$, it is enough to show that

$$\mathbf{F}^{\mathrm{J}}(K+1) \geq \mathbf{F}^{\mathrm{J}}(K). \tag{39}$$

Denote

$$\mathbf{B}_1(K) = \sum_{k=1}^{K} |S(\omega_k)|^2 \mathbf{t}^*(k)\mathbf{t}^T(k)$$

$$\mathbf{B}_2(K) = \sum_{k=1}^{K} \omega_k |S(\omega_k)|^2 \mathbf{t}^*(k)\mathbf{t}^T(k)$$

$$\mathbf{B}_3(K) = \sum_{k=1}^{K} \omega_k^2 |S(\omega_k)|^2 \mathbf{t}^*(k)\mathbf{t}^T(k)$$

and

$$\tilde{\mathbf{B}}_1(K) = \begin{bmatrix} \mathbf{B}_1(K) & \mathbf{B}_1(K) \\ \mathbf{B}_1(K) & \mathbf{B}_1(K) \end{bmatrix}, \quad \tilde{\mathbf{B}}_2(K) = \begin{bmatrix} \mathbf{B}_2(K) \\ \mathbf{B}_2(K) \end{bmatrix}.$$

First, similar to (37), the FIM $\mathbf{F}^{\mathrm{J}}(K)$ can be expressed as

$$\mathbf{F}^{\mathrm{J}}(K) = \frac{2}{\sigma^2} \Re\{\mathbf{M}_3 \odot \mathbf{M}_4 \odot \mathbf{M}_5(K)\}$$

where $\mathbf{M}_3$ is given by (37) and

$$\mathbf{M}_4 = \begin{bmatrix} \boldsymbol{\Psi}^H\boldsymbol{\Psi} & -j\boldsymbol{\Psi}^H\mathbf{A} & \boldsymbol{\Psi}^H\mathbf{A} & j\boldsymbol{\Psi}^H\mathbf{A} \\ j\mathbf{A}^H\boldsymbol{\Psi} & \mathbf{A}^H\mathbf{A} & j\mathbf{A}^H\mathbf{A} & -\mathbf{A}^H\mathbf{A} \\ \mathbf{A}^H\boldsymbol{\Psi} & -j\mathbf{A}^H\mathbf{A} & \mathbf{A}^H\mathbf{A} & j\mathbf{A}^H\mathbf{A} \\ -j\mathbf{A}^H\boldsymbol{\Psi} & -\mathbf{A}^H\mathbf{A} & -j\mathbf{A}^H\mathbf{A} & \mathbf{A}^H\mathbf{A} \end{bmatrix}$$

$$\mathbf{M}_5(K) = \begin{bmatrix} \tilde{\mathbf{B}}_1(K) & \tilde{\mathbf{B}}_2(K) & \tilde{\mathbf{B}}_1(K) \\ \tilde{\mathbf{B}}_2^H(K) & \mathbf{B}_3(K) & \tilde{\mathbf{B}}_2^H(K) \\ \tilde{\mathbf{B}}_1(K) & \tilde{\mathbf{B}}_2(K) & \tilde{\mathbf{B}}_1(K) \end{bmatrix}.$$

Then, to show (39), it is enough to show

$$\begin{aligned} &\mathbf{F}^{\mathrm{J}}(K+1) - \mathbf{F}^{\mathrm{J}}(K) \\ &= \frac{2}{\sigma^2} \Re\{\mathbf{M}_3 \odot \mathbf{M}_4 \odot [\mathbf{M}_5(K+1) - \mathbf{M}_5(K)]\} \\ &\geq \mathbf{0} \end{aligned} \tag{40}$$

Using the fact that $\Re\{\mathbf{M}\} \geq \mathbf{0}$ if $\mathbf{M} \geq \mathbf{0}$, it follows that (40) holds if

$$\mathbf{M}_3 \odot \mathbf{M}_4 \odot [\mathbf{M}_5(K+1) - \mathbf{M}_5(K)] \geq \mathbf{0}. \tag{41}$$

Since $\mathbf{M}_3 \geq \mathbf{0}$ (see Appendix B) and

$$\mathbf{M}_4 = \begin{bmatrix} \boldsymbol{\Psi}^H \\ j\mathbf{A}^H \\ \mathbf{A}^H \\ -j\mathbf{A}^H \end{bmatrix} [\boldsymbol{\Psi} \quad -j\mathbf{A} \quad \mathbf{A} \quad j\mathbf{A}]$$

is also positive semidefinite, it follows from the properties of Hadamard product that (41) holds if $\mathbf{M}_5(K+1) - \mathbf{M}_5(K) \geq \mathbf{0}$. Further, since

$$\begin{aligned} &\mathbf{M}_5(K+1) - \mathbf{M}_5(K) = |S(\omega_{K+1})|^2 \\ &\times \begin{bmatrix} \tilde{\mathbf{t}}^*(K+1) \\ \omega_k \mathbf{t}^*(K+1) \\ \tilde{\mathbf{t}}^*(K+1) \end{bmatrix} \left[\tilde{\mathbf{t}}^T(K+1) \;\; \omega_k \mathbf{t}^T(K+1) \;\; \tilde{\mathbf{t}}^T(K+1)\right] \end{aligned}$$

is positive semidefinite, the assertion (41) and further (39) are proved, which completes the proof.

REFERENCES

[1] C. Wu, Z. Yang, Z. Zhou, Y. Liu, and M. Liu, "Mitigating large errors in WiFi-based indoor localization for smartphones," *IEEE Trans. Vehicular Technology*, vol. 66, no. 7, pp. 6246–6257, July 2017.

[2] Z. Wu, K. Fu, E. Jedari, S. R. Shuvra, R. Rashidzadeh, and M. Saif, "A fast and resource efficient method for indoor positioning using received signal strength," *IEEE Trans. Vehicular Technology*, vol. 65, no. 12, pp. 9747–9758, 2016.

[3] J. Xiong and K. Jamieson, "Arraytrack: A fine-grained indoor location system," *10th USENIX Symposium on Networked Systems Design and Implementation (NSDI13)*, 2013, pp. 71–84.

[4] M. Koivisto, A. Hakkarainen, M. Costa, P. Kela, K. Leppanen, and M. Valkama, "High-efficiency device positioning and location-aware communications in dense 5G networks," *arXiv preprint*, arXiv:1608.03775, 2016.

[5] Z. Wu, Y. Han, Y. Chen, and K. J. R. Liu, "A time-reversal paradigm for indoor positioning system," *IEEE Trans. Vehicular Technology*, vol. 64, no. 4, pp. 1331–1339, 2015.

[6] D. Dardari, P. Closas, and P. M. Djuric, "Indoor tracking: Theory, methods, and technologies," *IEEE Trans. Vehicular Technology*, vol. 64, no. 4, pp. 1263–1278, Apr. 2015.

[7] M. Kotaru, K. Joshi, D. Bharadia, and S. Katti, "Spotfi: Decimeter level localization using wifi," *ACM SIGCOMM Computer Communication Review*, vol. 45, no. 4, pp. 26–282, 2015.

[8] M. Koivisto, M. Costa, J. Werner, K. Heiska, et al., "Joint device positioning and clock synchronization in 5G ultra-dense networks," *arXiv preprint*, arXiv:1604.03322, 2016.

[9] M. Koivisto, M. Costa, A. Hakkarainen, et al., "Joint 3D positioning and network synchronization in 5G ultra-dense networks using UKF and EKF," *arXiv preprint*, arXiv:1608.03710, 2016.

[10] M. Wax and A. Leshem, "Joint estimation of time delays and directions of arrival of multiple reflections of a known signal," *IEEE Trans. Signal Process.*, vol. 45, pp. 2477–2484, Oct. 1997.

[11] M. C. Vanderveen, C. B. Papadias, and A. J. Paulraj, "Joint angle and delay estimation (JADE) for multipath signals arriving at an antenna array," *IEEE Commun. Lett.*, vol. 1, no. 1, pp. 12–14, Jan. 1997.

[12] A. J. Van Der Veen, M. C. Vanderveen, and A. J. Paulraj, "Joint angle and delay estimation using shift-invariance properties," *IEEE Signal Processing Letters*, vol. 4, no. 5, pp. 142–145, 1997.

[13] A. Swindlehurst, "Time delay and spatial signature estimation using known asynchronous signals," *IEEE Trans. Signal Process.*, vol. 46, no. 2, pp. 449–462, Feb. 1998.

[14] G. G. Raleigh and T. Boros, "Joint space-time parameter estimation for wireless communication channels," *IEEE Trans. Signal Process.*, vol. 46, no. 5, pp. 1333–1343, May 1998.

[15] A. Van der Veen, M. C. Vanderveen, and A. Paulraj, "Joint angle and delay estimation using shift-invariance techniques," *IEEE Trans. Signal Process.*, vol. 46, no. 2, pp. 405–418, Feb. 1998.

[16] M. C. Vanderveen, A. Van der Veen, and A. Paulraj, "Estimation of multipath parameters in wireless communications," *IEEE Trans. Signal Process.*, vol. 46, no. 3, pp. 682–690, Mar. 1998.

[17] Y.-F. Chen and M. D. Zoltowski, "Joint angle and delay estimation for DS-CDMA with application to reduced dimension space-time RAKE receivers," *IEEE Trans. Acoust. Speech Signal Process.*, vol.5, pp. 2933–2936, March 1999.

[18] Y. Y. Wang, J. T. Chen, and W. H. Fang, "TST-MUSIC for joint DOA-delay estimation," *IEEE Trans. Signal Process.*, vol. 49, pp. 721–729, Apr. 2001.

[19] J. Picheral and U. Spagnolini, "Angle and delay estimation of space-time channels for TD-CDMA systems," *IEEE Trans. Wireless Commun.*, vol. 3, no. 3, pp. 758–769, May 2004.

[20] A. N. Lemma, A.-J. van der Veen, and E. F. Deprettere, "Analysis of joint angle-frequency estimation using ESPRIT," *IEEE Trans. Signal Process.*, vol. 51, pp. 1264–1283, May 2003.

[21] J. He, M. N. S. Swamy, and M. O. Ahmad, "Joint space-time parameter estimation for underwater communication channels with velocity vector sensor arrays," *IEEE Trans. Wireless Communications*, vol. 11, no. 11, pp. 3869–3877, Nov. 2012.

[22] A. Bazzi, D. T.M. Slock, and L. Meilhac, "Efficient maximum likelihood joint estimation of angles and times of arrival of multiple paths," in *Proc. of IEEE GLOBECOM Workshop on Localization for Indoors, Outdoors, and Emerging Networks*, 2015.

[23] A. Bazzi, D. T. M. Slock, and L. Meilhac, "On spatio-frequential smoothing for joint angles and times of arrival estimation of multipaths," *ICASSP*, 2016.

[24] F. Wen, Q. Wan, R. Fan, and H. W. Wei, "Improved MUSIC algorithm for multiple noncoherent subarrays," *IEEE Signal Process. Lett.*, vol. 21, no. 5, pp. 527–530, 2014.

[25] H. Krim and M. Viberg, "Two decades of array signal processing research: The parametric approach," *IEEE Signal Process. Mag.*, Vol.13, No.4, pp.67–94, 1996.

[26] W. Xie, F. Wen, J. Liu, and Q. Wan, "Source association, DOA and fading coefficients estimation for multipath signals," *IEEE Trans. Signal Process.*, vol. 65, no. 11, pp. 2773–2786, June 2017.

[27] I. Jaafar, H. Boujema, and M. Siala, "Joint azimuth, elevation and time of arrival estimation of 3-D Point sources," in *Proc. ISCCSP*, 2008, pp. 931–935.

[28] H. Wang and J.-K. Wang, "Joint two dimensional DOA and multipath time delay estimation in rectangular planar array," in *Proc. TENCON*, 2007, pp. 1–4.

[29] D. Alibi, U. Javed, et al., "2D DOA estimation method based on channel state information for uniform circular array," in *Proc. Int. Conf. Ubiquitous Positioning Indoor Navigation and Location Based Services (UPINLBS)*, 2016, pp. 68–72.

[30] A. Shaw and R. Kumaresan, "Frequency-wavenumber estimation by structured matrix approximation," in *Proc. IEEE Spectrum Estimation Workshop*, 1987, pp. 81–84.

[31] I. Ziskind and M. Wax, "Maximum likelihood localization of multiple sources by alternating projections," *IEEE Trans. Acoust., Speech, Signal Process.*, vol. 36, pp. 1553–1560, Oct. 1988.

[32] P. Stoica and A. Nehorai, "Music, maximum likelihood, and Cramer–Rao bound," *IEEE Trans. Acoust., Speech, Signal Process.*, vol. 37, pp. 720–743, May 1989.

[33] F. Wen and Q. Wan, "Maximum likelihood and signal-selective TDOA estimation for noncircular signals," *Journal of Communications and Networks*, vol. 15, no. 3, pp. 245–251, June 2013.

[34] Y. Shen and M. Z. Win, "Fundamental limits of wideband localizationł-Part I: A general framework," *IEEE Trans. Information Theory*, vol. 56, no.10, pp. 4956–4980, 2010.

[35] F. Wen, Q. Wan, and L. Y. Luo, "Time-difference-of-arrival estimation for noncircular signals using information theory," *Int. Journal Electronics Communications*, vol. 67, no. 3, pp. 242–245, 2013.

[36] P. Stoica and A. Nehorai, "Performance study of conditional and unconditional direction-of-arrival estimation," *IEEE Trans. Acoust. Speech, Signal Process.*, vol. 38, no. 10, pp. 1783–1795, Oct. 1990.

[37] M. Z. Win, A. Conti, S. Mazuelas, Y. Shen, et al, "Network localization and navigation via cooperation," *IEEE Communications Magazine*, vol. 49, no. 5, pp. 56–62, 2011.

[38] Y. Shen, S. Mazuelas, and M. Z. Win, "Network navigation: theory and interpretation," *IEEE Journal Selected Areas Communications*, vol. 30, no. 9, pp. 1823–1834, 2012.

[39] Y. Shen and M. Z. Win, "On the accuracy of localization systems using wideband antenna arrays," *IEEE Trans. Communications*, vol. 58, no. 1, pp. 270–280, 2010.

[40] S. Mazuelas, R. M. Lorenzo, A. Bahillo, et al, "Topology assessment provided by weighted barycentric parameters in harsh environment wireless location systems," *IEEE Trans. Signal Processing*, vol. 58, no. 7, pp. 3842–3857, 2010.

[41] L. Lu and H. Wu, "Novel robust direction-of-arrival-based source localization algorithm for wideband signals," *IEEE Trans. Wireless Communications*, vol. 11, no.11, pp. 3850–3859, 2012.